A quasi-onedimensional approach for hypersonic stagnation-point flows

Arno Klomfass [1]
Lehr- und Forschungsgebiet für Mechanik

Siegfried Müller
Institut für Geometrie und Praktische Mathematik

RWTH Aachen, 52056 Aachen

E-Mail: mueller@igpm.rwth-aachen.de or
klomfass@lufmech.rwth-aachen.de

Abstract

An approximate method for the efficient calculation of stagnation streamline quantities in hypersonic flows about spheres or cylinders is suggested. Based on the local similarity of the flow field the two-dimensional Navier-Stokes equations are simplified to a one-dimensional approximation for the stagnation streamline. The dimensionally reduced equations are solved with an implicit finite-volume scheme. Comparisons with fully two–dimensional Euler and Navier–Stokes calculations for flows about spheres are presented, that include perfect gas flows and flows in chemical non-equilibrium. Comparisons with a number of experiments conclude this report.

Key Words: Non-equilibrium, Stagnation Streamline, Local Similarity, Navier-Stokes equations, Chemically reacting flows.

AMS subject classification: 35Q30, 80A32, 76M20, 90C90

---

[1] The author is supported by the Deutsche Forschungsgemeinschaft

1 Notation

a_f	frozen speed of sound [m/s]
γ_f	ratio of frozen specific heats [-]
ρ_α	partial density of component α [kg/m^3]
ρ	density [kg/m^3]
$\underset{\sim}{v}$	velocity vector [m/s]
$\underset{\sim}{j}_\alpha$	diffusion flux vector of component α [kg/m^{2}s]
$\underset{\sim}{q}$	molecular heat flux vector [W/m^2]
ω_α	chemical production rate of component α [kg/m^3 s]
$\underset{\approx}{\tau}$	shear stress tensor [N/m^2]
p	hydrostatic pressure [N/m^2]
E	total energy [J/kg]
H	total enthalpy [J/kg]
e_α	specific energy of component α [J/kg]
h_α	specific enthalpy of component α [J/kg]
T_α^{vib}	vibrational temperature of component α [K]
T^{tr}	translational temperature [K]
x_α	mass fraction of component α [-]
y_α	mole fraction of component α [-]
D	diffusion coefficient $[kg/m^3s]$
μ	viscosity coefficient $[kg/ms]$
λ	heat-conduction coefficient $[W/mK]$

2 Introduction

The hypersonic flow about a spacecraft entering the atmosphere at orbital velocity is characterized by two main features: the high kinetic energy of the flow that leads to strong molecular collisions, and the low density of the atmosphere that results in small molecular collision rates. Molecular collisions with sufficient energy lead to the excitation of higher molecular modes, mainly vibration, and to changes in the gas composition as molecules dissociate. Due to small collision rates the chemical reactions and the energy exchange between the molecular modes have to be considered as finite-rate processes. Finite-rate processes become significant if the equilibration time of the energy distribution or the equilibration time of the chemical composition is comparable to the mean resident time of the gas in the flow field.

This non-equilibrium flow is described mathematically by the conservation equations for the mass, the momentum and the total energy of the gas mixture and additional balance equations for the partial densities of the components and the vibrational energies of the molecular components. The physical model enters these equations via the expressions for the chemical production rates, the energy exchange rates and the molecular fluxes.

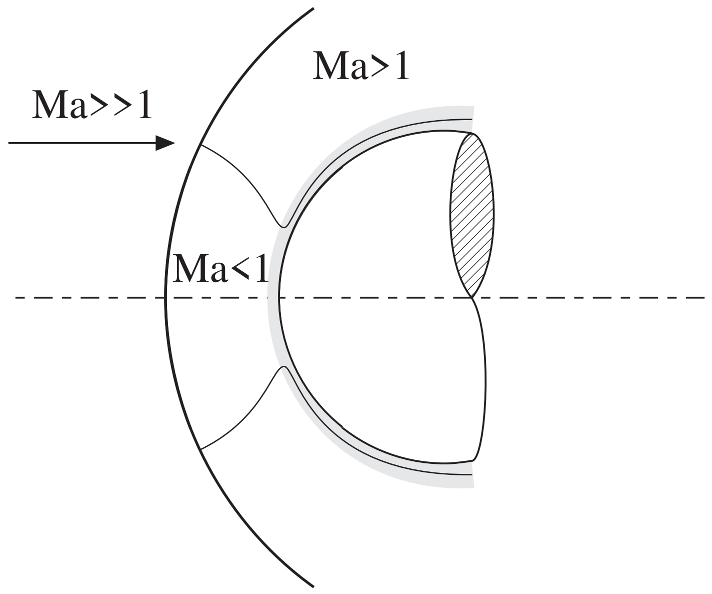

Figure 1: Hypersonic blunt body flow

The calculation of stagnation-streamline quantities in hypersonic flows about spheres and cylinders requires the solution of the governing equations with two independent spatial variables. The computational domain has to be extended at least beyond the boundaries of the subsonic region of the shock layer. The computation is thus rather time consuming and not suitable for parametric studies or a fast analysis of a specific flow situation.

In the approach suggested in this report the governing equations are simplified by reducing the number of independent spatial variables. This leads to a quasi one-dimensional approximation for the stagnation streamline in hypersonic flows about spheres and cylinders. The simplified set of equations, in the following called dimensionally reduced Navier-Stokes equations (DRNSE), can be solved numerically within some minutes on a standard workstation or PC, even with very high resolution. The DRNSE are based on the local similarity of the stagnation-streamline area in the considered flow fields. This local similarity has already been studied by several scientists, cf. [2], [6], [7], [8], [9], [10]. Numerical integration of similarly reduced equations has been attempted by Johnston and Hendricks [22] with however limited success.

The aim of this work is to provide a numerical tool for pre- and post-experimental analysis, examination of thermochemical models and the fast and reliable determination of stagnation-point heat fluxes. Within the present paper the DRNSE are validated against two-dimensional calculations for flows about spheres, where excatly the same physical model has been used. Furthermore, comparisons with the formula of Fay and Riddell for the stagnation-point heat flux and comparisons with experiments are presented.

3 Fluid dynamic balance equations

The volumetric balance equations for the masses of the chemical components, the momentum and the total energy of the gas mixture, and the vibrational energies of the molecular components are

$$
\begin{aligned}
\frac{\partial \rho_\alpha}{\partial t} + \operatorname{div}(\rho_\alpha \underset{\sim}{v}) + \operatorname{div}(\underset{\sim}{j}_\alpha) &= \omega_\alpha\,, & (1)\\
\frac{\partial \rho \underset{\sim}{v}}{\partial t} + \operatorname{div}(\rho \underset{\sim}{v} \circ \underset{\sim}{v} + p \underset{\approx}{E}) + \operatorname{div}(\underset{\approx}{\tau}) &= \underset{\sim}{0}\,, & (2)\\
\frac{\partial \rho E}{\partial t} + \operatorname{div}(\rho H \underset{\sim}{v}) + \operatorname{div}(\underset{\approx}{\tau}\underset{\sim}{v}) + \operatorname{div}(\underset{\sim}{q}) &= 0\,, & (3)\\
\frac{\partial \rho_\alpha e_\alpha^{(vib)}}{\partial t} + \operatorname{div}(\rho_\alpha e_\alpha^{(vib)} \underset{\sim}{v}) + \operatorname{div}(e_\alpha^{(vib)} \underset{\sim}{j}_\alpha + \underset{\sim}{q}_\alpha^{(vib)}) &= \Omega_\alpha^{(vib)}, & (4)
\end{aligned}
$$

where the density, the total specific energy and the total specific enthalpy are given by

$$
\rho = \sum_{\alpha=1}^{N} \rho_\alpha, \qquad E = e + \frac{\underset{\sim}{v}^2}{2}, \qquad H = E + p/\rho. \qquad (5)
$$

The balance equations (1) can be added up to obtain the mass conservation equation. As the sum of the diffusion fluxes and the sum of the species mass production vanish by definition, there is

$$
\frac{\partial \rho}{\partial t} + \operatorname{div}(\rho \underset{\sim}{v}) = 0. \qquad (6)
$$

If the gas composition is assumed constant or in local equilibrium, the set of balance equations (1) can be replaced by (6). If a flow with vibrational equilibrium or with frozen vibrational energies is assumed the balance equations (4) are dropped.

Relations for the molecular fluxes, i.e. the diffusion fluxes, the stress tensor, the vibrational heat fluxes and the total heat flux are obtained from a Chapman–Enskog expansion of the Boltzmann equation, cf.[1],

$$
\begin{aligned}
\underset{\sim}{j}_\alpha &= -D_\alpha \operatorname{grad} x_\alpha\,, & (7)\\
\underset{\approx}{\tau} &= -\mu \left\{ \operatorname{grad} \underset{\sim}{v} + (\operatorname{grad} \underset{\sim}{v})^T - \frac{2}{3}(\operatorname{div} \underset{\sim}{v}) \underset{\approx}{E} \right\}, & (8)\\
\underset{\sim}{q} &= -\lambda^{(1)} \operatorname{grad} T^{(tr)} + \sum_\alpha \underset{\sim}{q}_\alpha^{(vib)} + \sum_\alpha h_\alpha \underset{\sim}{j}_\alpha\,, & (9)\\
\underset{\sim}{q}_\alpha^{(vib)} &= -\lambda_\alpha^{(vib)} \operatorname{grad} T_\alpha^{(vib)}\,. & (10)
\end{aligned}
$$

Here bulk viscosity, pressure- and thermo-diffusion have been neglected. The relations are then essentially identical with the empirical approaches of Fick, Newton, and Fourier. Together with the balance equations (1) - (4) they form the Navier–Stokes equations for the non-equilibrium flow of a mixture of thermally perfect gases.

The purely algebraic relations for the pressure, the energies, and the transport coefficients are provided by constitutive relations given in Sec. 6.

It has to be noted, that the Navier–Stokes equations do not apply for flows with severe deviations from equilibrium. They fail to provide correct solutions for the structure of strong shock waves. The application is in practice limited to flows, where the thickness of the shock wave is small compared to the thickness of the shock layer.

We will now consider the balance equations in some more detail. The set of balance equations can formally be written as

$$\frac{\partial\,\mathbf{u}}{\partial\,t} + \mathrm{div}\,(\mathbf{F}_1^I, \mathbf{F}_2^I, \mathbf{F}_3^I) + \mathrm{div}\,(\mathbf{F}_1^V, \mathbf{F}_2^V, \mathbf{F}_3^V) = \mathbf{S}, \tag{11}$$

or in cartesian coordinates with $\underset{\sim}{x} = (x_1, x_2, x_3)^T$ as

$$\frac{\partial\,\mathbf{u}}{\partial\,t} + \sum_{i=1}^{3} \frac{\partial\,\mathbf{F}_i^I}{\partial\,x_i} + \sum_{i=1}^{3} \frac{\partial\,\mathbf{F}_i^V}{\partial\,x_i} = \mathbf{S}, \tag{12}$$

where $\mathbf{u}$ denotes the volume-specific balance quantities, $\mathbf{F}_i^I$ the inviscid fluxes, $\mathbf{F}_i^V$ the viscous fluxes and $\mathbf{S}$ the source terms.

$$\mathbf{u} = \begin{pmatrix} \rho_1 \\ \vdots \\ \rho_N \\ \rho \underset{\sim}{v} \\ \rho E \\ \rho_1 e_1^{(vib)} \\ \vdots \\ \rho_M e_M^{(vib)} \end{pmatrix}, \mathbf{S} = \begin{pmatrix} \omega_1 \\ \vdots \\ \omega_N \\ \underset{\sim}{0} \\ 0 \\ \Omega_1^{(vib)} \\ \vdots \\ \Omega_M^{(vib)} \end{pmatrix},$$

$$\mathbf{F}_i^I = \begin{pmatrix} \rho_1 v_i \\ \vdots \\ \rho_N v_i \\ \rho \underset{\sim}{v} v_i + p \underset{\sim}{e}_i \\ \rho v_i H \\ \rho_1 e_1^{(vib)} v_i \\ \vdots \\ \rho_1 e_M^{(vib)} v_i \end{pmatrix}, \mathbf{F}_i^V = \begin{pmatrix} \underset{\sim}{j}_1 \underset{\sim}{e}_i \\ \vdots \\ \underset{\sim}{j}_N \underset{\sim}{e}_i \\ \underset{\approx}{\tau} \underset{\sim}{e}_i \\ (\underset{\sim}{q} + \underset{\approx}{\tau} \underset{\sim}{v}) \underset{\sim}{e}_i \\ (e_1^{(vib)} \underset{\sim}{j}_1 + \underset{\sim}{q}_1^{(vib)}) \underset{\sim}{e}_i \\ \vdots \\ (e_M^{(vib)} \underset{\sim}{j}_M + \underset{\sim}{q}_M^{(vib)}) \underset{\sim}{e}_i \end{pmatrix}.$$

Here $\underset{\sim}{e}_i$ is the i-th unit vector in the three dimensional space. The chemical components are arranged such that the molecular components are enumerated from 1 to M and the atomic components from $M+1$ to N.

The balance equations (1) - (4), and the molecular fluxes (7) - (9) are obtained in specific coordinates when the respective contravariant basis vectors are introduced into the definitions of the gradient and the divergence operators,

$$\operatorname{grad}\varphi = \sum_{\lambda=1}^{3} \frac{\partial\,\varphi}{\partial\,x^\lambda} \circ \underset{\sim}{g}^\lambda, \quad \operatorname{div}\varphi = \sum_{\lambda=1}^{3} \frac{\partial\,\varphi}{\partial\,x^\lambda} \cdot \underset{\sim}{g}^\lambda,$$

where $\varphi = \varphi(t, \underset{\sim}{x})$ may be either a scalar, a vector or a tensor. In the next two sections spherical and cylindrical coordinates are considered. The major part of the formulas given there is quoted from [5]. More details about the coordinate transformation are given in App. 10.1.

4 Derivation of the DRNSE

To derive the DRNSE the original equations are first cast in spherical or cylindrical coordinates for the rotationally symmetric or plane flow problem, respectively, as is shown in sec. 4.1 and 4.2. A separation of variables technique is then applied to a suitable set of flow quantities. These flow quantities are represented as products of unknown functions of the radial coordinate and prescribed functions of the angular coordinate. The differentiation with respect to the angular coordinate can then be carried out to obtain the DRNSE. The success of this approach of course depends on the choice of the flow quantities and the choosen dependencies of the angular coordinate. Details will be given in Sec. 4.3.

4.1 Spherical coordinates

The arrangement of the spherical coordinates (r, θ, ϕ) is illustrated in Fig. 2. Since we are dealing with rotationally symmetric problems, we can directly take into account, that $\partial/\partial\phi = 0$ and $v_\phi = 0$ if the direction of the undisturbed flow is the z-axis ($\theta = 0$) in Fig. 2. The application of the divergence operator to a scalar p, a vector $\underset{\sim}{v}$ and a tensor $\underset{\approx}{\tau}$ then leads to the following relations, cf. [5], pp. 739C - 739D,

$$\operatorname{div}(\underset{\approx}{E}p)\,|_r = p_{,r}\,, \tag{13}$$

$$\operatorname{div}(\underset{\approx}{E}p)\,|_\theta = \frac{1}{r}p_{,\theta}\,, \tag{14}$$

$$\operatorname{div}(\underset{\sim}{v}) = v_{r,r} + \frac{2}{r}v_r + \frac{\cot\theta}{r}v_\theta + \frac{1}{r}v_{\theta,\theta}\,, \tag{15}$$

$$\operatorname{div}(\underset{\approx}{\tau})\,|_r = \tau_{rr,r} + \frac{2}{r}\tau_{rr} + \frac{\cot\theta}{r}\tau_{r\theta} + \frac{1}{r}\tau_{r\theta,\theta} - \frac{1}{r}\tau_{\theta\theta} - \frac{1}{r}\tau_{\phi\phi}\,, \tag{16}$$

$$\operatorname{div}(\underset{\approx}{\tau})\,|_\theta = \tau_{r\theta,r} + \frac{3}{r}\tau_{r\theta} + \frac{\cot\theta}{r}\tau_{\theta\theta} + \frac{1}{r}\tau_{\theta\theta,\theta} - \frac{\cot\theta}{r}\tau_{\phi\phi}\,. \tag{17}$$

The symbols $|_r$ and $|_\theta$ denote the $r-$ and $\theta-$components of the respective vectors. The above relations can directly be introduced into the original balance equations. The above used vector $\underset{\sim}{v}$ can also be identified with $\rho\underset{\sim}{v}$, $\underset{\approx}{\tau}\underset{\sim}{v}$, $\underset{\sim}{q}$, $\underset{\sim\alpha}{q}^{(vib)}$, $\underset{\sim\alpha}{j}$ to obtain the respective

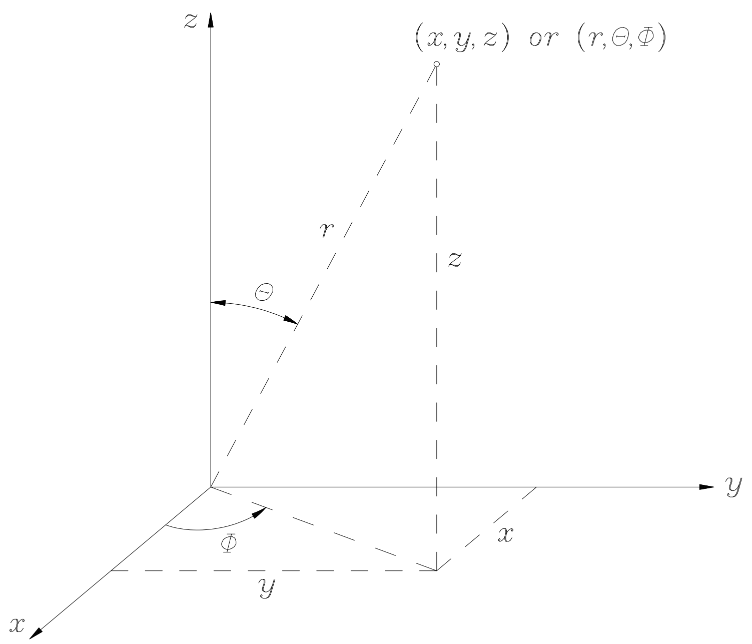

Figure 2: Spherical coordinates

expressions in spherical coordinates. In the same manner the above relation for the tensor $\underset{\approx}{\tau}$ can be applied to $\rho \underset{\sim}{v} \circ \underset{\sim}{v}$ to get

$$\operatorname{div}(\rho \underset{\sim}{v} \circ \underset{\sim}{v})|_r = (\rho v_r v_r)_{,r} + \frac{2}{r}(\rho v_r v_r) + \frac{\cot\theta}{r}(\rho v_r v_\theta) + \frac{1}{r}(\rho v_r v_\theta)_{,\theta} - \frac{1}{r}(\rho v_\theta v_\theta)\,, \tag{18}$$

$$\operatorname{div}(\rho \underset{\sim}{v} \circ \underset{\sim}{v})|_\theta = (\rho v_r v_\theta)_{,r} + \frac{3}{r}(\rho v_r v_\theta) + \frac{\cot\theta}{r}(\rho v_\theta v_\theta) + \frac{1}{r}(\rho v_\theta v_\theta)_{,\theta}\,. \tag{19}$$

The elements of the stress tensor are again taken from [5], pp. 90.

$$\tau_{rr} = -\mu \left\{ \frac{4}{3} v_{r,r} - \frac{4}{3}\frac{v_r}{r} - \frac{2}{3}\frac{\cot\theta}{r} v_\theta - \frac{2}{3}\frac{v_{\theta,\theta}}{r} \right\}, \tag{20}$$

$$\tau_{r\theta} = -\mu \left\{ -\frac{1}{r} v_\theta + v_{\theta,r} + \frac{1}{r} v_{r,\theta} \right\}, \tag{21}$$

$$\tau_{\theta\theta} = -\mu \left\{ -\frac{2}{3} v_{r,r} + \frac{2}{3}\frac{v_r}{r} + \frac{4}{3}\frac{v_{\theta,\theta}}{r} - \frac{2}{3}\frac{\cot\theta}{r} v_\theta \right\}, \tag{22}$$

$$\tau_{\phi\phi} = -\mu \left\{ -\frac{2}{3} v_{r,r} + \frac{2}{3}\frac{v_r}{r} + \frac{4}{3}\frac{\cot\theta}{r} v_\theta - \frac{2}{3}\frac{v_{\theta,\theta}}{r} \right\}. \tag{23}$$

4.2 Cylindrical coordinates

The arrangement of the cylindrical coordinates (r, ϕ, z) is illustrated in Fig. 3. Here we consider a plane, two-dimensional flow, where the free-stream direction is the $x-$axis $(\theta = 0)$. With $\partial/\partial z = 0$ and $v_z = 0$ the application of the divergence operator to a scalar p, a vector $\underset{\sim}{v}$ and a tensor $\underset{\approx}{\tau}$ leads to the following relations, cf. [5], pp. 739. The elements

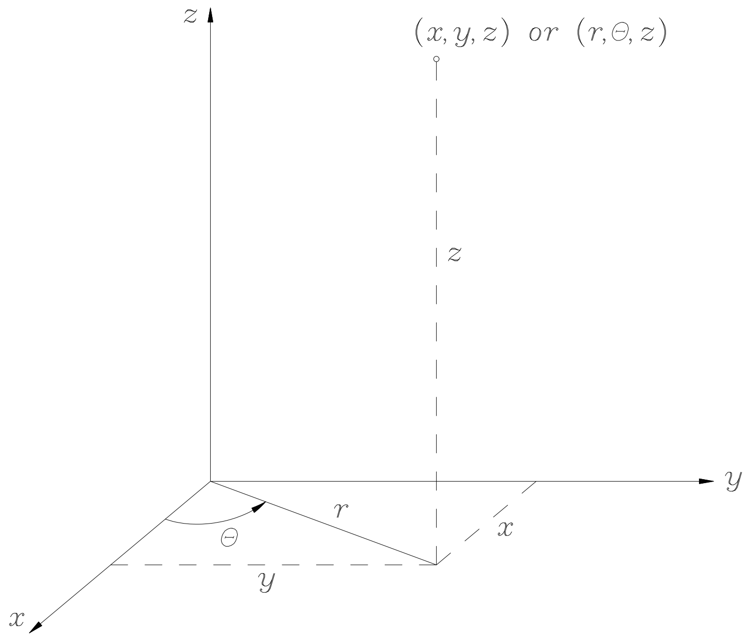

Figure 3: Cylindrical coordinates

of the stress tensor are as before taken from [5], pp. 89.

$$
\begin{aligned}
\mathrm{div}\,(\underset{\approx}{E}p)\,|_r &= p_{,r}\,, && (24)\\
\mathrm{div}\,(\underset{\approx}{E}p)\,|_\theta &= \frac{1}{r}p_{,\theta}\,, && (25)\\
\mathrm{div}\,(\underset{\sim}{v}) &= v_{r,r} + \frac{1}{r}v_r + \frac{1}{r}v_{\theta,\theta}\,, && (26)\\
\mathrm{div}\,(\underset{\approx}{\tau})\,|_r &= \tau_{rr,r} + \frac{1}{r}\tau_{rr} + \frac{1}{r}\tau_{r\theta,\theta} - \frac{1}{r}\tau_{\theta\theta}\,, && (27)\\
\mathrm{div}\,(\underset{\approx}{\tau})\,|_\theta &= \tau_{r\theta,r} + \frac{2}{r}\tau_{r\theta} + \frac{1}{r}\tau_{\theta\theta,\theta}\,, && (28)\\
\mathrm{div}\,(\rho\underset{\sim}{v}\circ\underset{\sim}{v})\,|_r &= (\rho v_r v_r)_{,r} + \frac{1}{r}(\rho v_r v_r) + \frac{1}{r}(\rho v_r v_\theta)_{,\theta} - \frac{1}{r}(\rho v_\theta v_\theta)\,, && (29)\\
\mathrm{div}\,(\rho\underset{\sim}{v}\circ\underset{\sim}{v})\,|_\theta &= (\rho v_r v_\theta)_{,r} + \frac{2}{r}(\rho v_r v_\theta) + \frac{1}{r}(\rho v_\theta v_\theta)_{,\theta}\,, && (30)\\
\tau_{rr} &= -\mu\left\{\frac{4}{3}v_{r,r} - \frac{2}{3}\frac{v_r}{r} - \frac{2}{3}\frac{v_{\theta,\theta}}{r}\right\}\,, && (31)\\
\tau_{r\theta} &= -\mu\left\{-\frac{1}{r}v_\theta + v_{\theta,r} + \frac{1}{r}v_{r,\theta}\right\}\,, && (32)\\
\tau_{\theta\theta} &= -\mu\left\{-\frac{2}{3}v_{r,r} + \frac{4}{3}\frac{v_r}{r} + \frac{4}{3}\frac{v_{\theta,\theta}}{r}\right\}\,. && (33)\\
& && (34)
\end{aligned}
$$

4.3 Ansatz for the DRNSE

In deriving the DRNSE we assume, that a suitable set of flow quantities $\mathbf{f}$ can be expressed, at least approximately, by a separation of variables technique, i.e.

$$\mathbf{f}(r,\theta) = \mathbf{f}^*(\theta)\,\bar{\mathbf{f}}(r). \tag{35}$$

This approach can also be looked at as a special case of an asymptotic expansion and some comments about this will be given at the end of this section.

In our approach we prescribe the functional dependencies $\mathbf{f}^*(\theta)$ on the basis of intuitive arguments. To derive a physically meaningful approximation several constraints for the possible choices for $\mathbf{f}^*(\theta)$ have to be considered. These constraints arise from geometrical-, symmetry- and boundary-conditions.

The symmetry of the flow field implies that the quantities $v_r,\ p,\ T, x_\alpha$ are symmetric to the axis $\theta = 0$. In contrast, the angular velocity component v_θ behaves anti-symmetric. The undisturbed parallel supersonic free-stream is a boundary condition the ansatz should satisfy. If an isothermal, fully catalytic wall is considered the temperatures and mass fractions are constant along the surface. In a first approximation it may thus be assumed, that these quantities are a function of the radial coordinate alone. As a further condition we introduce the Newtonian theory that provides the approximation

$$p_w - p_\infty = \frac{1}{2}\rho_\infty v_\infty \cos^2\theta \tag{36}$$

for the surface pressure in the hypersonic limit, i.e. when $Ma \to \infty$, cf. [11]. This is a useful approximation even at finite Mach numbers $Ma \gg 1$, provided the bow shock is about concentric to the sphere or cylinder surface, respectively. In view of these constraints, the following ansatz seems promising:

$$\begin{aligned}
v_r &= \overline{v}_r(r)\cos\theta\,, \\
v_\theta &= \overline{v}_\theta(r)\sin\theta\,, \\
p - p_\infty &= \overline{p}(r)\cos^2\theta\,, \\
T^{(tr)} &= \overline{T}^{(tr)}(r)\,, \\
T_\alpha^{(vib)} &= \overline{T}_\alpha^{(vib)}(r)\,, \\
x_\alpha &= \overline{x}_\alpha(r)\,.
\end{aligned}$$

It should be noted, that the ansatz for the temperatures and the mass fractions is less favorable if an adiabatic or non-catalytic wall is considered, respectively. Furthermore, the ansatz fails to provide a correct description for the temperature behind the shock, which of course depends on the shock angle. This may however be tolerated as the main interest focuses on the boundary layer part of the flow field. In terms of the chosen ansatz, the boundary conditions are

$$\text{Free}-\text{stream}:\left\{\begin{array}{lcl}\overline{p} & = & 0\\ \overline{v}_r & = & u_\infty\\ \overline{T}^{(tr)} & = & T_\infty^{(tr)}\\ \overline{v}_\theta & = & u_\infty\\ \overline{T}_\alpha^{(vib)} & = & T_{\alpha\infty}^{(vib)}\\ \overline{x}_\alpha & = & x_{\alpha,\infty}\end{array}\right. \quad \text{Stagn.}-\text{point}:\left\{\begin{array}{lclclcl}\overline{p}_{,r} & = & 0 & & & & \\ \overline{v}_r & = & 0 & & & & \\ \overline{T}^{(tr)} & = & T_W^{(tr)} & & & & \\ \overline{v}_\theta & = & 0 & or & \overline{v}_{\theta,r} & = & 0\\ \overline{T}_\alpha^{(vib)} & = & T_{\alpha W}^{(vib)} & or & \overline{T}_{\alpha,r}^{(vib)} & = & 0\\ \overline{x}_\alpha & = & x_{\alpha,W} & or & \overline{x}_{\alpha,r} & = & 0\end{array}\right.$$

These boundary conditions describe the supersonic parallel free stream, a no-slip or slip wall, an isothermal or adiabatic wall, and a fully catalytic or a non-catalytic wall.

Remarks about asymptotic expansion: If we consider only the shock layer part of the flow field, or flow fields with shocks of finite thickness, all flow quantities are differentiable. We can thus expand the flow quantities in the vicinity of the stagnation streamline $\theta = 0$ in a Taylor series. This can be done in such a way, that the coefficients depend on the radial coordinate alone. To achieve this we first expand the considered function f in the point (x_0, z_0):

$$f(x,z) = \sum_{i,j=0}^{\infty} \frac{1}{i!j!} \left.\frac{\partial^{i+j} f}{\partial x^i \, \partial z^j}\right|_{(x_0,z_0)} (x-x_0)^i (z-z_0)^j .$$

In spherical coordinates x, x_0, z and z_o are given as

$$x = r\cos\theta,\ \ z = r\sin\theta,\ \ x_0 = r\cos\theta_0,\ \ z_0 = r\sin\theta_0 .$$

For $\theta_0 \to 0$ the serie reduces to

$$f(x,z) = \sum_{i,j=0}^{\infty} f_{ij}(r)(\cos\theta - 1)^i (\sin\theta)^j \tag{37}$$

with

$$f_{ij}(r) = \frac{1}{i!j!} \left.\frac{\partial^{i+j} f}{\partial x^i \, \partial z^j}\right|_{(r,0)} r^{i+j} .$$

Application of the binomial formula to the term $(\cos\theta - 1)^i$ renders after rearranging the summation order

$$f(x,z) = \sum_{l,j=0}^{\infty} \overline{f}_{lj}(r)(\cos\theta)^l (\sin\theta)^j \tag{38}$$

with

$$\overline{f}_{lj}(r) = \sum_{i=l}^{\infty} \binom{i}{l} f_{ij}(r)(-1)^{i-l} .$$

This technique is frequently applied to the analysis of the stagnation streamline flow, cf. [2], [8], [10], [9]. Substituting the Taylor series for the chosen quantities into the balance equations and evaluating the derivatives with respect to the angular coordinate renders an infinite set of differential equations for the coefficients. The expansion is then truncated in such a way that a closed system with a finite number of equations remains.

4.4 DRNSE for spheres

Substituting the above Ansatz into the relations (13) to (23) given in sec. 4.1 yields

$$
\begin{aligned}
\mathrm{div}\,(\underset{\approx}{E}p)\,|_r &= \overline{p}_{,r}\cos^2\theta\,, & (39)\\
\mathrm{div}\,(\underset{\approx}{E}p)\,|_\theta &= -\frac{2}{r}\overline{p}\cos\theta\sin\theta\,, & (40)\\
\mathrm{div}\,(\underset{\sim}{v}) &= \left(\overline{v}_{r,r}+\frac{2}{r}\overline{v}_r+\frac{2}{r}\overline{v}_\theta\right)\cos\theta\,, & (41)\\
\mathrm{div}\,(\rho\underset{\sim}{v}\circ\underset{\sim}{v})\,|_r &= \left((\rho\overline{v}_r\overline{v}_r)_{,r}+\frac{2}{r}(\rho\overline{v}_r\overline{v}_r)+\frac{2}{r}(\rho\overline{v}_r\overline{v}_\theta)\right)\cos^2\theta\,, & (42)\\
\mathrm{div}\,(\rho\underset{\sim}{v}\circ\underset{\sim}{v})\,|_\theta &= \left((\rho\overline{v}_r\overline{v}_\theta)_{,r}+\frac{3}{r}(\rho\overline{v}_r\overline{v}_\theta)+\frac{3}{r}(\rho\overline{v}_\theta\overline{v}_\theta)\right)\cos\theta\sin\theta\,, & (43)\\
\tau_{rr} &= \overline{\tau}_{rr}\cos\theta = -\mu\left\{\frac{4}{3}\overline{v}_{r,r}-\frac{4}{3}\frac{\overline{v}_r}{r}-\frac{4}{3}\frac{\overline{v}_\theta}{r}\right\}\cos\theta\,, & (44)\\
\tau_{r\theta} &= \overline{\tau}_{r\theta}\sin\theta = -\mu\left\{-\frac{1}{r}\overline{v}_\theta+\overline{v}_{\theta,r}-\frac{1}{r}\overline{v}_r\right\}\sin\theta\,, & (45)\\
\tau_{\theta\theta} &= \tau_{\phi\phi} = -\frac{1}{2}\tau_{rr}\,, & (46)\\
\mathrm{div}\,(\underset{\approx}{\tau})\,|_r &= \left(\overline{\tau}_{rr,r}+\frac{2}{r}\overline{\tau}_{rr}+\frac{2}{r}\overline{\tau}_{r\theta}-\frac{2}{r}\overline{\tau}_{\theta\theta}\right)\cos\theta\,, & (47)\\
\mathrm{div}\,(\underset{\approx}{\tau})\,|_\theta &= \left(\overline{\tau}_{r\theta,r}+\frac{3}{r}\overline{\tau}_{r\theta}-\frac{1}{r}\overline{\tau}_{\theta\theta}\right)\sin\theta\,, & (48)\\
j_{\alpha r} &= -D_\alpha x_{\alpha,r}\,,\quad j_{\alpha\theta}=0\,, & (49)\\
q_r &= -\lambda^{(1)}T^{(tr)}_{,r}-\sum_\alpha\lambda^{(vib)}_\alpha T^{(vib)}_{\alpha,r}+\sum_\alpha j_{\alpha r}h_\alpha\,,\quad q_\theta=0\,. & (50)
\end{aligned}
$$

In the expressions for $\rho\underset{\sim}{v}\circ\underset{\sim}{v}$ terms with coefficients $\sin\theta$, or higher powers of $\sin\theta$ have been neglected, as they are small against the remaining terms, as $\theta\to0$.

Considering the equation of the angular momentum, we notice that $\sin\theta$ can be factorized. In a final step the equations are now specified for the stagnation streamline by letting $\theta\to0$. This limiting process renders the DRNSE which can be written formally as

$$\overline{\mathbf{u}}_{,t}+\overline{\mathbf{F}}^I_{,r}+\overline{\mathbf{F}}^V_{,r}+(\overline{\mathbf{G}}^I+\overline{\mathbf{G}}^V)\,r^{-1}=\mathbf{S},$$

$$\overline{\mathbf{u}} = \begin{pmatrix} \rho_1 \\ \vdots \\ \rho_N \\ \rho\overline{v}_r \\ \rho\overline{v}_\theta \\ \rho E \\ \rho_1 e_1^{(vib)} \\ \vdots \\ \rho_M e_M^{(vib)} \end{pmatrix}, \overline{\mathbf{F}}^I = \begin{pmatrix} \rho_1\overline{v}_r \\ \vdots \\ \rho_N\overline{v}_r \\ \rho\overline{v}_r^2 + p \\ \rho\overline{v}_r\overline{v}_\theta \\ \rho\overline{v}_r H \\ \rho_1 e_1^{(vib)}\overline{v}_r \\ \vdots \\ \rho_M e_M^{(vib)}\overline{v}_r \end{pmatrix}, \overline{\mathbf{F}}^V = \begin{pmatrix} j_{r1}^D \\ \vdots \\ j_{rN}^D \\ \overline{\tau}_{rr} \\ \overline{\tau}_{r\theta} \\ q_r + \overline{\tau}_{rr}\overline{v}_r \\ e_1^{(vib)} j_{r1} + q_{r1}^{(vib)} \\ \vdots \\ e_M^{(vib)} j_{rM} + q_{rM}^{(vib)} \end{pmatrix},$$

$$\overline{\mathbf{G}}^I = \begin{pmatrix} 2\,\rho_1(\overline{v}_r + \overline{v}_\theta) \\ \vdots \\ 2\,\rho_N(\overline{v}_r + \overline{v}_\theta) \\ 2\,\rho\overline{v}_r(\overline{v}_r + \overline{v}_\theta) \\ 3\,\rho\overline{v}_\theta(\overline{v}_r + \overline{v}_\theta) - 2\,\overline{p} \\ 2\,\rho H(\overline{v}_r + \overline{v}_\theta) \\ 2\,\rho_1 e_1^{(vib)}(\overline{v}_r + \overline{v}_\theta) \\ \vdots \\ 2\,\rho_M e_M^{(vib)}(\overline{v}_r + \overline{v}_\theta) \end{pmatrix}, \overline{\mathbf{G}}^V = \begin{pmatrix} 2\,j_{r1} \\ \vdots \\ 2\,j_{rN} \\ 2\,(\overline{\tau}_{rr} - \overline{\tau}_{\theta\theta} + \overline{\tau}_{r\theta}) \\ -\overline{\tau}_{\theta\theta} + 3\,\overline{\tau}_{r\theta} \\ 2(q_r + \overline{\tau}_{rr}\overline{v}_r + \overline{\tau}_{r\theta}\overline{v}_r + \overline{\tau}_{\theta\theta}\overline{v}_\theta) \\ 2(e_1^{(vib)} j_{r1} + q_{r1}^{(vib)}) \\ \vdots \\ 2(e_M^{(vib)} j_{rM} + q_{rM}^{(vib)}) \end{pmatrix}.$$

It should be noted, that both the inviscid and viscous metric terms $\overline{\mathbf{G}}^I$, $\overline{\mathbf{G}}^V$ consist of two contributions. One arises from the introduction of the spherical coordinates in the balance equations and another from the evaluation of the derivatives with respect to θ in the context of the DRNSE approximation. The source terms in the DRNSE are unaltered against the original expressions.

4.5 DRNSE for cylinders

The procedures are identical with those presented in the preceeding section. The results are thus presented without further comments.

$$\begin{aligned}
\operatorname{div}(\underset{\approx}{E}p)\,|_r &= \overline{p}_{,r}\cos^2\theta && (51)\\
\operatorname{div}(\underset{\approx}{E}p)\,|_\theta &= -\frac{2}{r}\overline{p}\cos\theta\sin\theta && (52)\\
\operatorname{div}(\underset{\sim}{v}) &= \left(\overline{v}_{r,r} + \frac{1}{r}\overline{v}_r + \frac{1}{r}\overline{v}_\theta\right)\cos\theta && (53)\\
\operatorname{div}(\rho\underset{\sim}{v}\circ\underset{\sim}{v})\,|_r &= \left((\rho\overline{v}_r\overline{v}_r)_{,r} + \frac{1}{r}(\rho\overline{v}_r\overline{v}_r) + \frac{1}{r}(\rho\overline{v}_r\overline{v}_\theta) - \frac{\tan^2\theta}{r}\rho\overline{v}_\theta(\overline{v}_r + \overline{v}_\theta)\right)\cos^2\theta && (54)\\
\operatorname{div}(\rho\underset{\sim}{v}\circ\underset{\sim}{v})\,|_\theta &= \left((\rho\overline{v}_r\overline{v}_\theta)_{,r} + \frac{2}{r}(\rho\overline{v}_r\overline{v}_\theta) + \frac{2}{r}(\rho\overline{v}_\theta\overline{v}_\theta)\right)\cos\theta\sin\theta && (55)
\end{aligned}$$

$$\tau_{rr} = \overline{\tau}_{rr}\cos\theta = -\mu\left\{\frac{4}{3}\overline{v}_{r,r} - \frac{2}{3}\frac{\overline{v}_r}{r} - \frac{2}{3}\frac{\overline{v}_\theta}{r}\right\}\cos\theta \tag{56}$$

$$\tau_{r\theta} = \overline{\tau}_{r\theta}\sin\theta = -\mu\left\{-\frac{1}{r}\overline{v}_\theta + \overline{v}_{\theta,r} - \frac{1}{r}\overline{v}_r\right\}\sin\theta \tag{57}$$

$$\tau_{\theta\theta} = \overline{\tau}_{\theta\theta}\cos\theta = -\mu\left\{-\frac{2}{3}\overline{v}_{r,r} + \frac{4}{3}\frac{\overline{v}_r}{r} + \frac{4}{3}\frac{\overline{v}_\theta}{r}\right\}\cos\theta \tag{58}$$

$$\operatorname{div}(\underset{\approx}{\tau})|_r = \left(\overline{\tau}_{rr,r} + \frac{1}{r}\overline{\tau}_{rr} + \frac{1}{r}\overline{\tau}_{r\theta} - \frac{1}{r}\overline{\tau}_{\theta\theta}\right)\cos\theta \tag{59}$$

$$\operatorname{div}(\underset{\approx}{\tau})|_\theta = \left(\overline{\tau}_{r\theta,r} + \frac{2}{r}\overline{\tau}_{r\theta} - \frac{1}{r}\overline{\tau}_{\theta\theta}\right)\sin\theta \tag{60}$$

$$\tag{61}$$

$$\overline{\mathbf{u}} = \begin{pmatrix} \rho_1 \\ \vdots \\ \rho_N \\ \rho\overline{v}_r \\ \rho\overline{v}_\theta \\ \rho E \\ \rho_1 e_1^{(vib)} \\ \vdots \\ \rho_M e_M^{(vib)} \end{pmatrix}, \overline{\mathbf{F}}^I = \begin{pmatrix} \rho_1\overline{v}_r \\ \vdots \\ \rho_N\overline{v}_r \\ \rho\overline{v}_r^2 + p \\ \rho\overline{v}_r\overline{v}_\theta \\ \rho\overline{v}_r H \\ \rho_1 e_1^{(vib)}\overline{v}_r \\ \vdots \\ \rho_M e_M^{(vib)}\overline{v}_r \end{pmatrix}, \overline{\mathbf{F}}^V = \begin{pmatrix} j_{r1}^D \\ \vdots \\ j_{rN}^D \\ \overline{\tau}_{rr} \\ \overline{\tau}_{r\theta} \\ q_r + \overline{\tau}_{rr}\overline{v}_r \\ e_1^{(vib)} j_{r1} + q_{r1}^{(vib)} \\ \vdots \\ e_M^{(vib)} j_{rM} + q_{rM}^{(vib)} \end{pmatrix}$$

$$\overline{\mathbf{G}}^I = \begin{pmatrix} \rho_1(\overline{v}_r + \overline{v}_\theta) \\ \vdots \\ \rho_N(\overline{v}_r + \overline{v}_\theta) \\ \rho\overline{v}_r(\overline{v}_r + \overline{v}_\theta) \\ 2\,\rho\overline{v}_\theta(\overline{v}_r + \overline{v}_\theta) - 2\,\overline{p} \\ \rho H(\overline{v}_r + \overline{v}_\theta) \\ \rho_1 e_1^{(vib)}(\overline{v}_r + \overline{v}_\theta) \\ \vdots \\ \rho_M e_M^{(vib)}(\overline{v}_r + \overline{v}_\theta) \end{pmatrix}, \overline{\mathbf{G}}^V = \begin{pmatrix} j_{r1} \\ \vdots \\ j_{rN} \\ \overline{\tau}_{rr} - \overline{\tau}_{\theta\theta} + \overline{\tau}_{r\theta} \\ -\overline{\tau}_{\theta\theta} + 2\,\overline{\tau}_{r\theta} \\ q_r + \overline{\tau}_{rr}\overline{v}_r + \overline{\tau}_{r\theta}\overline{v}_r + \overline{\tau}_{\theta\theta}\overline{v}_\theta \\ e_1^{(vib)} j_{r1} + q_{r1}^{(vib)} \\ \vdots \\ e_M^{(vib)} j_{rM} + q_{rM}^{vib} \end{pmatrix}.$$

5 The numerical method

An implicit time integration method is applied to obtain steady-state solutions of the DRNSE, which are approximated by the finite-volume equations

$$\frac{\overline{\mathbf{u}}_i^{n+1} - \overline{\mathbf{u}}_i^n}{\Delta t} + \frac{\overline{\mathbf{F}}_{i+1/2}^{n+1} - \overline{\mathbf{F}}_{i-1/2}^{n+1}}{\Delta r} + \overline{\mathbf{G}}_i^{n+1} = \mathbf{S}_i^{n+1}\,, \tag{62}$$

with $\Delta t = t^{n+1} - t^n$ and $\Delta r = (r_{i+1} - r_{i-1})/2$. In the above notation, both the viscous and inviscid contributions to the fluxes and metric terms are included in $\overline{\mathbf{F}}$ and $\overline{\mathbf{G}}$.

The viscous fluxes at the cell interfaces $i \pm 1/2$ and the cell centers i are approximated by second order accurate finite differences as functions of the respective values at points $i-1, i$ and $i+1$. The inviscid fluxes at the cell interfaces are approximated by the averages of the inviscid fluxes at points $i-1, i$ and $i, i+1$, respectively. The finite-volume approximation is thus second order accurate in space and exactly identical to a centered finite-difference approximation.

The unknowns $\overline{\mathbf{u}}^{n+1}$, $\overline{\mathbf{F}}^{n+1}$, $\overline{\mathbf{G}}^{n+1}$ and $\mathbf{S}^{n+1}$ at time $t^{n+1} = t^n + \Delta t$ are extrapolated from their values at time t^n by means of a truncated taylor expansion. For $\mathbf{q}$ being any of the above quantities there is

$$\mathbf{q}^{n+1} = \mathbf{q}^n + \left.\frac{\partial\,\mathbf{q}}{\partial\,\mathbf{w}}\right|^n \Delta\mathbf{w}^n \ , \ \ \Delta\mathbf{w}^n = \mathbf{w}^{n+1} - \mathbf{w}^n \, . \tag{63}$$

At this stage primitive variables $\mathbf{w}$ are introduced:

$$\mathbf{w} = \left(\overline{v}_r, \overline{v}_\theta, \overline{T}^{(tr)}, \overline{p}, \overline{x}_\alpha, \overline{T}^{(vib)}_\alpha\right)^T \, .$$

The use of primitive variables as dependent variables is not strictly necessary. It however simplifies the incorporation of the boundary conditions and the derivation of the jacobians $\partial\mathbf{q}/\partial\mathbf{w}$ considerably, especially the viscous parts of it. Introducing (63) into (62) and rearranging terms renders

$$\mathbf{a}_i \Delta\mathbf{w}^n_{i-1} + \mathbf{b}_i \Delta\mathbf{w}^n_i + \mathbf{c}_i \Delta\mathbf{w}^n_{i+1} = -\left(\overline{\mathbf{F}}^n_{i+1/2} - \overline{\mathbf{F}}^n_{i-1/2} + \Delta r \overline{\mathbf{G}}^n_i - \Delta r \mathbf{S}^n_i\right) \, , \tag{64}$$

$$\begin{aligned}
\mathbf{c}_i &= \frac{\partial\,\overline{\mathbf{F}}^n_{i+1/2}}{\partial\,\mathbf{w}_{i+1}} - \frac{\partial\,\overline{\mathbf{F}}^n_{i-1/2}}{\partial\,\mathbf{w}_{i+1}} + \frac{\partial\,\overline{\mathbf{G}}^n_i}{\partial\,\mathbf{w}_{i+1}}\Delta r \, , \\
\mathbf{a}_i &= \frac{\partial\,\overline{\mathbf{F}}^n_{i+1/2}}{\partial\,\mathbf{w}_{i-1}} - \frac{\partial\,\overline{\mathbf{F}}^n_{i-1/2}}{\partial\,\mathbf{w}_{i-1}} + \frac{\partial\,\overline{\mathbf{G}}^n_i}{\partial\,\mathbf{w}_{i-1}}\Delta r \, , \\
\mathbf{b}_i &= \frac{\partial\,\overline{\mathbf{F}}^n_{i+1/2}}{\partial\,\mathbf{w}_i} - \frac{\partial\,\overline{\mathbf{F}}^n_{i-1/2}}{\partial\,\mathbf{w}_i} + \frac{\partial\,\overline{\mathbf{G}}^n_i}{\partial\,\mathbf{w}_i}\Delta r - \frac{\partial\,\mathbf{S}^n_i}{\partial\,\mathbf{w}_i}\Delta r + \frac{\partial\,\overline{\mathbf{u}}^n_i}{\partial\,\mathbf{w}_i}\frac{\Delta r}{\Delta t} \, .
\end{aligned}$$

The whole set of equations for the interior points $i = 2, \ldots, N-1$ of the computational domain can be written in matrix notation as

$$\mathbf{A}^n \Delta\mathbf{w}^n = \mathbf{RHS}^n \, , \tag{65}$$

where $\mathbf{A}$ is a square block-tridiagonal matrix. In this notation the products $\mathbf{a}_2\Delta\mathbf{w}^n_1$ and $\mathbf{c}_{N-1}\Delta\mathbf{w}^n_N$ that contain the boundary values $\mathbf{w}_1$ and $\mathbf{w}_N$ are included on the right hand side. Dirichlet boundary conditions are incorporated by assigning the desired value to the respective variables w_1 or w_N and setting the corresponding Δw_1 or Δw_N to zero. Neuman boundary conditions, which are relevant for the stagnation-point ($i = 1$), are approximated by finite differences and expressed in terms of Δw^n, i.e.

$$w^{n+1}_{1,r} = 0 = \frac{4}{3}\Delta w^n_2 - \frac{1}{3}\Delta w^n_3 - \Delta w^n_1 + \frac{4}{3}w^n_2 - \frac{1}{3}w^n_3 - w^n_1 \, . \tag{66}$$

This relation is added to equation (65) to eliminate the unknown Δw_1^n. Note, that the above relation holds for an equidistant grid only.

Steady-state solutions are obtained asymptotically by successive evaluations of (65). The iteration scheme is formally identical with a Newton-Raphson iteration that makes the right hand side zero, which corresponds here to the conservative steady-state flow equations. Due to the implicit formulation timesteps with large Courant numbers can be realized and a few hundert steps are usually sufficient to obtain a practically converged solution. The computation is initialized with $\mathbf{w}_i, i = 1, N$ interpolated linearly between free-stream and stagnation-point conditions, where part of the latter have to be guessed.

In each time step, the block-tridiagonal system of equations (65) has to be solved for $\Delta\mathbf{w}^n$. A Gaussian elemination with pivoting is used for this task. In the elemination, the block-tridiagonal structure of the matrix is taken into account to achieve a short computation time.

The above finite-volume approximation is appropriate for low Reynolds-number flows, where the molecular fluxes are significant and thick shock waves exist. Solutions with thin shock waves cannot be obtained with this method, due to the central approximation of the inviscid fluxes. For these cases a shock-fitting strategy is used.

5.1 Shock-fitting procedure

If shock-fitting is applied, the computational domain contains only the shock-layer part of the stagnation streamline. As the steady-state shock position is a priori unknown, it is calculated simultaneously with the shock-layer flow. For given initial data at t^n the shock position at t^{n+1} is determined from the shock speed. The computational grid is then fitted to the new shock position and the finite-volume equations are evaluated with the post-shock conditions at t^{n+1} as upstream boundary conditions ($i = N$). As the changes in shock position per timestep are negligible compared to the shock layer thickness, the same balance equations for stationary control volumes are used.

The shock speed and the post-shock conditions are determined from the Rankine-Hugoniot relations (RHR), an additional compatibility relation (CR) and the constituitive relations. For a chemically and vibrationally frozen gas the RHR are

$$\begin{aligned} [v_t] &= 0\,, && (67)\\ [\rho(v_n - V_s)] &= 0\,, && (68)\\ [\rho(v_n - V_s)^2 + p] &= 0\,, && (69)\\ [h + \frac{1}{2}(v_n - V_s)^2] &= 0\,, && (70)\\ [x_\alpha] &= 0\,, && (71) \end{aligned}$$

$$[e_\alpha^{(vib)}] = 0\,. \tag{72}$$

If thermal equilibrium is considered the equation $[e_\alpha^{(vib)}] = 0$ is dropped from the RHR. The shock-normal and -tangential base vectors $\underset{\sim}{g}_n$ and $\underset{\sim}{g}_t$ define the velocity components

$$v_t = \underset{\sim}{v}\underset{\sim}{g}_t \quad , \quad v_n = \underset{\sim}{v}\underset{\sim}{g}_n \, , \quad V_s = \underset{\sim}{v}_s\underset{\sim}{g}_n \quad , \tag{73}$$

where $\underset{\sim}{V}_s$ denotes the shock speed. The flow velocities v_n and v_t are here identical with v_r and v_θ as the shock front is normal to the stagnation streamline.

The post-shock conditions can be calculated from the RHR if shock speed and upstream flow conditions are given. The shock speed itself has to be iterated until the post-shock conditions satisfy the discretized compatibility relation $\mathcal{F} = 0$,

$$\mathcal{F} = \Delta_B^S p - [a_f \rho]_B^S \, \Delta_B^S v_r + [a_f^2 \rho \frac{v_{\theta,\theta}}{r}]_B^S \, \delta t + \Phi_B^C \tag{74}$$

The CR has been derived from the two-dimensional, unsteady Euler equations by [24]. It describes the propagation of a sound wave along the left-running characteristic that intersects the shock at $t^n + \delta t$, as is illustrated in Fig. 4. In (74) the Δ-operator denotes the

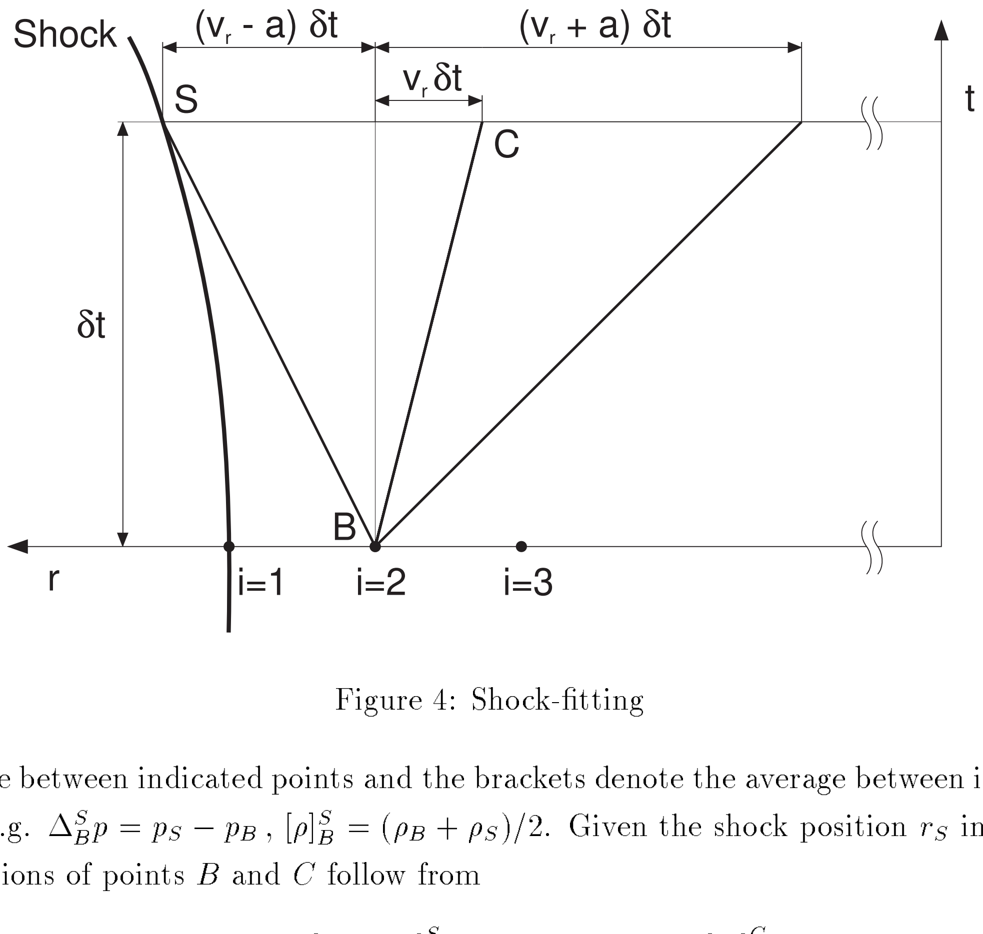

Figure 4: Shock-fitting

difference between indicated points and the brackets denote the average between indicated points, e.g. $\Delta_B^S p = p_S - p_B$, $[\rho]_B^S = (\rho_B + \rho_S)/2$. Given the shock position r_S in $t^n + \delta t$, the positions of points B and C follow from

$$r_B = r_S - [v_r - a_f]_B^S \, \delta t \, , \qquad r_C = r_B + [v_r]_B^C \, \delta t \, . \tag{75}$$

In the DRNSE-ansatz the shock is assumed concentric to the spherical or cylindrical body and the cross-derivative in (74) is thus given as $v_{\theta,\theta} = \overline{v}_\theta$. The relaxation term Φ is defined as

$$\Phi = [(\gamma_f - 1)\rho] \left\{ \sum_\alpha \Delta e_\alpha^{(vib)} + \sum_\alpha \left[e_\alpha^{(0)} + e_\alpha^{(1)} - \frac{R_\alpha T^{(tr)}}{\gamma_f - 1} \right] \Delta x_\alpha \right\} . \tag{76}$$

The superscript 1 denotes the group of molecular or atomic modes that are governed by the translational temperature, see Sec. 6. The relaxation term is evaluated between the points B and C, i.e. along the material pathline. As the conditions in point C at $t^n + \delta t$ are unknown at the time of calculation, the values from the corresponding point at time t^n are used as an approximation. This approach provides second order accuracy in the steady-state solution.

The iteration of the shock speed that renders $\mathcal{F} = 0$ is here achieved with the method of bisection. Within this iteration a local time step δt is applied, as indicated above. This time step is chosen as to make point B identical with the grid point $i = 2$ next to the shock. Once the shock speed is determined the shock position is updated with the global time step Δt.

Shock slip is not taken into account here, i.e. the molecular fluxes are not included in the RHR. This approximation is sufficiently accurate for high to moderate Reynolds-number flows, where the molecular fluxes immediately behind the shock are negligible compared to the macroscopic fluxes.

6 Constitutive relations

We consider air as a mixture of the five components N_2, O_2, NO, N and O, which are assumed to be thermally perfect gases. The pressure is thus given by

$$p = \sum_\alpha p_\alpha = \sum_\alpha \frac{2}{3} \rho_\alpha e_\alpha^{(tr)} = \sum_\alpha \rho_\alpha R_\alpha T^{(tr)} . \tag{77}$$

The internal energy of a component is assumed to consist of independent translational, electronic, rotational and vibrational contributions and the (positive) dissociation energy $e_\alpha^{(0)}$, i.e.

$$e_\alpha = e_\alpha^{(tr)} + e_\alpha^{(el)} + e_\alpha^{(rot)} + e_\alpha^{(vib)} - e_\alpha^{(0)} \quad , \tag{78}$$

where the last three terms are identical zero for atomic components.

The model of a rigidly rotating and harmonically vibrating molecule is used, with $e_\alpha^{(0)}$ as maximum vibrational energy, cf.[14], pp. 76. It is assumed, that individual Boltzmann distributions exist for each mode. The specific energies of these modes can then be described in terms of independent temperatures by caloric equations of state. These are obtained from partition functions, cf.[15], [14].

Here, a common temperature $T^{(tr)}$ is assigned to all translational, rotational and electronic modes. Independent temperatures $T_{N_2}^{(vib)}$, $T_{O_2}^{(vib)}$ and $T_{NO}^{(vib)}$ are introduced for the vibrational modes of the molecular components. If flows in thermal equilibrium are considered a common temperature T is assigned to all modes.

The chemical production rates ω_α are calculated from rate equations,

$$\omega_\alpha = M_\alpha \sum_r \left(\nu_\alpha^{(r'')} - \nu_\alpha^{(r')}\right) \left\{ k^{(r')} \prod_\beta (c_\beta)^{\nu_\beta^{(r')}} - k^{(r'')} \prod_\beta (c_\beta)^{\nu_\beta^{(r'')}} \right\} , \tag{79}$$

where $\nu_\alpha^{(r')}$ and $\nu_\alpha^{(r'')}$ denote the stoichometric coefficients that define the reactions r. The preferential dissociation model of Treanor and Marrone [16] is applied for the rate constants $k^{(r')}$ of the endothermic reactions, i.e.

$$k^{(r')} = \Psi_\alpha \, \tilde{k}^{(r')}(T^{(tr)}) . \tag{80}$$

Here, $\tilde{k}^{(r')}$ denotes the rate constants in thermal equilibrium. The preferential dissociation parameter Ψ_α accounts for the effect of vibrational non-equilibrium of the respective molecular reactant. It is given in terms of the vibrational partition function $Q_\alpha^{(vib)}$ as

$$\Psi_\alpha = \frac{Q_\alpha^{(vib)}(\ T^*\ )}{Q_\alpha^{(vib)}(T_\alpha^{(vib)})} \frac{Q_\alpha^{(vib)}(T^{(tr)})}{\theta_\alpha^0/\theta_\alpha^{(vib)}} , \quad \frac{1}{T_\alpha^*} = \frac{1}{T_\alpha^{(vib)}} - \frac{1}{T^{(tr)}} , \tag{81}$$

where $\theta_\alpha^0 = e_\alpha^0/k$ is the characteristic temperature associated with the dissociation energy and $\theta_\alpha^{(vib)}$ the characteristic temperature of vibration. In thermal equilibrium the parameter becomes unity. For $T_\alpha^{(vib)} < T^{(tr)}$ it is $\Psi_\alpha < 1$ and vice versa, so that the reaction is slowed down or speeded up depending on the temperatures. The rate constants of the endothermic reactions are deduced from the principle of detailled balance, i.e.

$$k^{(r'')} = \tilde{k}^{(r')}(T^{(tr)}) \,/\, K_r(T^{(tr)}) \quad \text{(recombination)}, \tag{82}$$

$$k^{(r'')} = \Psi_\alpha \, \tilde{k}^{(r')}(T^{(tr)}) \,/\, K_r(T^{(tr)}) \quad \text{(exoth. exchange reactions)} . \tag{83}$$

The equilibrium constants K_r are given in terms of the partition functions of the species associated with the respective reaction, cf.[14].

If vibrational non-equilibrium is considered, relations for the volume specific rates $\Omega_\alpha^{(vib)}$ of vibrational energy exchange are required, which are discussed next. The energy exchange in non-reactive molecular collisions mainly consists of VT and VV contributions, which are in the case of a harmonic oscillator model, cf.[21],

$$\Omega_{\alpha\beta}^{(VT)} = \rho_\alpha c_\beta \, k_{\alpha\beta}^{VT} \left(1 - \exp\left(-\theta_\alpha^{(vib)}/T^{(tr)}\right)\right) \left\{ e_\alpha^{(vib)}(T^{(tr)}) - e_\alpha^{(vib)} \right\} , \tag{84}$$

$$\begin{aligned} \Omega_{\alpha\beta}^{(VV)} = \rho_\alpha c_\beta \, k_{\alpha\beta}^{VV} \frac{1}{R_\beta \theta_\beta^{(vib)}} \Bigg\{ & \left(e_\alpha^{(vib)} + R_\alpha \theta_\alpha^{(vib)}\right) e_\beta^{(vib)} \exp\left(-\frac{\theta_\alpha^{(vib)} - \theta_\beta^{(vib)}}{T^{(tr)}}\right) \\ & - \left(e_\beta^{(vib)} + R_\beta \theta_\beta^{(vib)}\right) e_\alpha^{(vib)} \Bigg\} . \end{aligned} \tag{85}$$

The fundamental rate constants $k^{VT}_{\alpha\beta}$ are here calculated from curve fits to experimental data, cf.[24], while the $k^{VV}_{\alpha\beta}$ are obtained from the following heuristic relation, which acceptably fits the few available experimental data, cf.[24],

$$k^{VV}_{\alpha\beta} = \sqrt{k^{VT}_{\alpha\alpha}\, k^{VT}_{\beta\beta}\ \exp\left\{(\theta^{(vib)}_{\alpha} - \theta^{(vib)}_{\beta})/T^{(tr)}\right\}} . \tag{86}$$

The vibrational energy exchange in reactiv molecular collisions can be determined consistent with the preferrential dissociation theory. The volume specific rate of vibrational energy loss due to a dissociation or exchange reaction is then

$$\Omega^{(vib,diss)}_{\alpha} = \omega^{(diss)}_{\alpha}\, e^{(vib)}_{\alpha}(T^{*}_{\alpha}) . \tag{87}$$

In thermodynamic equilibrium there is $\Omega^{(vib,diss)}_{\alpha} = \Omega^{(vib,form)}_{\alpha}$, $\omega^{(r')}_{\alpha} = \omega^{(r'')}_{\alpha}$, and $T^{(vib)}_{\alpha} = T^{(tr)}$. The average vibrational energy of the molecules formed in a reaction is thus

$$e^{(vib,form)}_{\alpha} = \lim_{T^{*}_{\alpha}\to\infty} e^{(vib)}_{\alpha}(T^{*}_{\alpha}) = \frac{1}{2} R_{\alpha} \left(\theta^{(0)}_{\alpha} - \theta^{(vib)}_{\alpha}\right) . \tag{88}$$

Examination of the partition function shows, that the distribution of vibrational energy among the formed molecules is in this case a statistical one, i.e. each vibrational energy level has the same probability. Consequently, there is a random recombination in contrast to the preferential dissociation. It is assumed, that this holds in a non-equilibrium environment as well. The volume specific rates of reactiv vibrational energy gain is thus

$$\Omega^{(vib,form)}_{\alpha} = \omega^{(form)}_{\alpha} \frac{1}{2} R_{\alpha} \left(\theta^{(0)}_{\alpha} - \theta^{(vib)}_{\alpha}\right) . \tag{89}$$

More details about the thermochemical model are found in [24].

The viscosity μ of the gas mixture is approximated by the viscosities μ_{α} of the pure species and the mixing rule of Herning and Zipperer,

$$\mu = \sum_{\alpha=1}^{N} \frac{\mu_{\alpha} y_{\alpha}}{\phi_{\alpha}} \quad , \quad \phi_{\alpha} = \sum_{\beta} y_{\beta} \sqrt{M_{\beta}/M_{\alpha}} , \tag{90}$$

where y denotes mole fractions and M_{α} molar masses, cf.[20]. The viscosities of the pure species are calculated from the curve fits of Metz, which are based on experimental and theoretical data, cf.[3].

Finally, the heat conduction and diffusion coefficients are approximated by assumed constant Prandtl and Schmidt numbers, and the generalized Eucken correction of Hirschfelder, cf.[23],

$$\lambda^{1} = \frac{c^{1}_{p}\,\mu}{Pr} \quad , \quad D_{\alpha\beta} = D = \frac{\mu}{\rho Sc} \quad , \quad \lambda^{(vib)}_{\alpha} = x_{\alpha} c^{(vib)}_{v\alpha} \rho D . \tag{91}$$

where values of 0.7 have been used for either number Pr and Sc. The superscript 1 again denotes the group of molecular and atomic modes that are governed by the translational temperature. A further discussion of the molecular-flux model is found in [25].

7 Results and Discussion

At the present stage neither flows about cylinders nor flows in vibrational nonequilibrium have been examined. In the following we will thus focus on flows about spheres and especially on flows of a perfect gas and flows in chemical nonequilibrium.

To assess the accuracy of the DRNSE three sets of test cases are considered. The first two sets cover generic flows of a perfect gas and some generic high-enthalpy flows in chemical nonequilibrium. The third set contains a number of high-enthalpy flows, for which experimental results are available.

The accuracy of the DRNSE is assessed by comparisons with two-dimensional Euler and Navier-Stokes calculations on the basis of two issues: the shock standoff-distance and the stagnation-point heat-flux.

In the test cases 1.1 to 1.20 a perfect gas is considered, with $R = 289$ J/kgK, $\gamma = 1.4$, viscosity according to Sutherland's law, cf. [11], and a constant Prandtl number of 0.7. The sphere radius is 0.1 m and the wall temperature is 300 K. Viscous flows ranging from Mach number 2 to 50 with Reynolds numbers of 1000 to 1.0×10^6 have been calculated with the DRNSE-method for perfect gas. It has to be noted that these test cases are more or less without physical relevance due to the perfect gas model. They serve as purely numerical tests.

Two-dimensional inviscid reference-solutions are obtained from the Euler-scheme described in [24]. Reference values for the stagnation-point heat-fluxes have been determined with the formula of Fay and Riddell [12]. The conditions at the outer edge of the boundary layer, which are required in this formula, have been identified with the adiabatic stagnation-point conditions predicted by the Euler calculations (cf. App. 10.2, Tab. 6, 7). For the perfect gas there is no question concerning the thermochemical equilibration of the boundary layer. Fay and Riddell's formula can be employed without further assumptions.

Computational results for these test cases are summarized in Tab. 1. There are only five different Euler calculations, which render the shock-standoff distances in the inviscid flows. In all test cases, the free-stream temperature was 300 K. The Mach and Reynolds numbers have been tuned via the free-stream values of velocity and density. Given Reynolds numbers are based on the sphere diameter. As the Stanton number,

$$St = \frac{q}{\rho_\infty V_\infty (H_\infty - H_w)} \quad , \tag{92}$$

is a dimension-free quantity it depends on Mach and Reynolds number only if γ and Pr are considered fixed. From dimensional analysis it can further be seen that the Stanton number itself is proportional to $1/\sqrt{Re}$. Thus the stagnation-point heat-fluxes are proportional to $\sqrt{Re}$ in test cases 1.1 to 1.20.

		DRNSE			Euler/Fay&Riddell		rel.deviation	
#	Ma	Re	q [kW/m^2]	δ/R_{sph}	q [kW/m^2]	δ/R_{sph}	Δ q /q	$\Delta\delta/\delta$
1.1	2	1.E3	2.775	0.2615	2.719	0.3383	0.0206	-0.21
1.2	5	1.E3	32.34	0.1357	32.13	0.1559	0.0065	-0.13
1.3	10	1.E3	213.3	0.1115	189.5	0.1350	0.1260	-0.17
1.4	20	1.E3	1316	0.1008	1141	0.1299	0.1530	-0.22
1.5	50	1.E3	16380	0.0917	12560	0.1284	0.3040	-0.28
1.6	2	1.E4	8.458	0.2565	8.599	0.3383	-0.0164	-0.24
1.7	5	1.E4	95.4	0.1387	101.1	0.1559	-0.0602	-0.11
1.8	10	1.E4	592.4	0.1208	599.3	0.1350	-0.0115	-0.10
1.9	20	1.E4	3687	0.1148	3608	0.1299	0.0219	-0.11
1.10	50	1.E4	40330	0.1101	39710	0.1284	0.0156	-0.14
1.11	2	1.E5	26.17	0.2547	27.19	0.3383	-0.0375	-0.24
1.12	5	1.E5	295.4	0.1391	321.3	0.1559	-0.0806	-0.11
1.13	10	1.E5	1848	0.1227	1895	0.1350	-0.0248	-0.09
1.14	20	1.E5	11430	0.1182	11410	0.1299	-0.0018	-0.09
1.15	50	1.E5	120000	0.1161	125600	0.1284	-0.0446	-0.09
1.16	2	1.E6	83.5	0.2546	85.99	0.3383	0.0289	-0.24
1.17	5	1.E6	936.3	0.1392	1016	0.1559	-0.0748	-0.11
1.18	10	1.E6	6004	0.1232	5993	0.1350	0.0018	-0.09
1.19	20	1.E6	36460	0.1190	36080	0.1299	0.0105	-0.08
1.20	50	1.E6	37130	0.1177	397100	0.1284	-0.0650	-0.08

Table 1: Test cases 1.1 - 1.20: Results

The following conclusions can be derived from the computed results. First, the shock standoff-distance is always underestimated by the DRNSE. The deviation increases with decreasing Mach number or increasing shock standoff-distance. This behaviour may be attributed to the assumption of a newtonian-like pressure distribution, which holds respectively for high Mach numbers or small shock standoff-distances only. Second, the stagnation-streamline heat-fluxes deviate to about 8% from the results obtained with the formula of Fay and Riddell. It has to be noted however, that the latter itself is only a correlation to numerical solutions and does not provide exact results. Exceptions to these conclusions are found in test cases 1.3 to 1.5. In these cases the boundary-layer extents over a significant portion of the shock layer and increases with Mach number. Fay and Riddell's formula is therefore not applicable in the above mentioned way.

In the test cases 2.1 to 2.6 five-component air-flows in chemical nonequilibrium have been investigated. The respective free-stream conditions are summarized in Tab. 2. Given Reynolds numbers are here based on the sphere radius. A non-catalytic wall has been assumed througout. The DRNSE results are here compared to two-dimensional Navier-Stokes calculations based on a finite-volume scheme (cf. [26], [27], [28]), where an identical thermochemical model has been used. The grid resolution is about 120×130 equidistant

#	T_w [K]	R_{sph}[m]	V[m/s]	p[Pa]	T[K]	Ma	Re	x_{N_2}	x_{O_2}	x_{NO}	x_N	x_O
2.1	1500	0.1524	7600	4.18	212	26.0	22980	0.7654	0.2345	1E-5	1E-5	1E-5
2.2	1500	0.1524	7600	40.3	264	23.3	151700	0.7654	0.2345	1E-5	1E-5	1E-5
2.3	1500	0.1524	4100	75.9	270	12.4	148460	0.7654	0.2345	1E-5	1E-5	1E-5
2.4	1500	0.1524	4100	276	251	12.9	613800	0.7654	0.2345	1E-5	1E-5	1E-5
2.5	300	0.05	3568	90.2	196	12.7	87280	0.7654	0.2345	1E-5	1E-5	1E-5
2.6	300	0.05	2500	90.2	196	12.7	61160	0.7654	0.2345	1E-5	1E-5	1E-5

Table 2: Free stream conditions 2.1 - 2.6

points in the 2D-calculations and up to about 2000 equidistant points in the converged DRNSE solutions. Typical CPU times are 8 h for the 2D-method and 5 min for the DRNSE-scheme on a SGI workstation (IRIS–Indigo–R8000).

Results for the temperature and the mass fractions of the molecular species at the stagnation streamline are shown in Fig. 5 to Fig. 22. For test case 2.6 no mass fractions are shown, as the flow is chemically frozen. The employed methods provide qualitatively identical results in all test cases. As in the previous set of test cases the tendency of the DRNSE to underpredict the shock standoff-distance is observed. The relative deviations are here however smaller, as the shock standoff-distances are small in comparison with perfect-gas flows. Note that in case 2.1 the smeared shock could be captured with the DRNSE-scheme, while in the other cases shock-fitting was required. Some notable deviations were observed in the vicinity of the stagnation point in test case 2.2 to 2.4 which may be attributed to a nonsufficient resolution in the two-dimensional calculations. This becomes apparent in Figs. 9, 17 and 21. For these test cases deviations are also observed in the calculated stagnation-point heat-fluxes, which are listed in Tab. 3. For cases 2.1, 2.5 and 2.6 the agreement of the heat-fluxes is satisfactory.

	DRNSE		DRNSE (Euler b/c)/Fay&Riddell		2D-NS	
#	q [MW/m^2]	δ/R$_{sph}$	q_{fr} [MW/m^2]	q_{eq} [MW/m^2]	q [MW/m^2]	δ/R$_{sph}$
2.1	1.093	0.070	0.91	2.06	1.125	0.074
2.2	2.064	0.058	1.45	4.67	2.349	0.060
2.3	0.526	0.081	0.49	0.86	0.675	0.087
2.4	1.079	0.076	0.85	1.65	1.580	0.081
2.5	1.338	0.092	1.27	1.58	1.343	0.097
2.6	0.493	0.105	0.50	0.50	0.548	0.114

Table 3: Test cases 2.1 to 2.6: Results

As the Fay and Riddell formula covers only the limits of frozen and equilibrium boundary layers, its application provides only estimates for the lower and upper limits of the stagnation-point heat-fluxes, which are also listed in Tab. 3. The results are based on adiabatic stagnation-point conditions that have been determined from the DRNSE with Euler boundary-conditions. More details about these conditions are given in App. 10.2.

In the third set of test cases, Tab. 4, comparisons are made with experimentally determined heat fluxes. Heat fluxes and free-stream conditions for test cases 3.1 to 3.6 have been provided by Wen and Hornung [4]. Note that 3.5 and 3.6 are pure nitrogen flows. Traces of other components have been added for numerical reasons only. Test cases 3.7 to 3.9 have been examined at the TH2 shock-tube at Aachen by several investigators [29], [30]. Finally 3.10 and 3.11 are results from recent calibration-runs at the HEG facility at DLR Göttingen, [30], [31]. Fixed surface temperatures of 300 K have been assumed for all test cases. The DRNSE-scheme has here been used to calculate the stagnation-point heat-fluxes for the non-catalytic and the fully-catalytic surface. Results are summarized in Tab. 5.

#	T_w	R_{sph}	V	p	T	Ma	Re	x_{N_2}	x_{O_2}	x_{NO}	x_N	x_O
3.1	300	0.0381	3965	12407	1402	5.4	345200	0.7350	0.1730	0.06499	1E-5	0.0270
3.2	300	0.0254	3929	11180	1371	5.4	213400	0.7350	0.1730	0.06499	1E-5	0.0270
3.3	300	0.0254	5301	13090	2359	5.2	119920	0.7410	0.0580	0.03400	1E-5	0.1669
3.4	300	0.0381	5631	13835	2707	5.1	155400	0.7550	0.0230	0.02200	1E-5	0.1999
3.5	300	0.0254	4860	11930	1946	5.4	153400	0.9599	1E-5	1E-5	4E-2	1E-5
3.6	300	0.0381	5144	13530	2200	5.4	223300	0.9599	1E-5	1E-5	4E-2	1E-5
3.7	300	0.0125	2490	3400	345	6.7	217600	0.7654	0.2345	1E-5	1E-5	1E-5
3.8	300	0.0125	3470	9240	853	6.0	175720	0.7654	0.2345	1E-5	1E-5	1E-5
3.9	300	0.0500	3568	90.2	196	12.7	87300	0.7654	0.2345	1E-5	1E-5	1E-5
3.10	300	0.0100	5919	430	790	9.7	11300	0.7490	0.0360	0.03339	1E-5	0.1816
3.11	300	0.0100	4813	470	553	9.9	19990	0.7324	0.1444	0.06899	1E-5	0.0542

Table 4: Free stream conditions 3.1 - 3.11

For test cases 3.1 to 3.9 the DRNSE-results for the stagnation-point heat-fluxes are about the same for catalytic and non-catalytic surfaces. This indicates that the flow fields are close to local equilibrium. The experimental data match with the majority of the DRNSE-results very well (cf. Tab. 5).

It can be observed that the calculated stagnation-point heat-fluxes for the non-catalytic surface are somewhat closer to the experimentally measured values. A larger deviation is found in case 3.7. The flow in this test case is chemically almost frozen and is thus comparable to the flows in test cases 1.12 and 1.13, where the DRNSE performed well against the reference-solutions. The discrepancy observed here can not be explained yet.

The flow fields resulting from test conditions 3.10 and 3.11 are dominated by non-equilibrium effects, as is indicated by the large differences between the non-catalytic and fully catalytic cases. Large differences are also observed in the stagnation enthalpies, which depend on the gas composition alone as the wall temperatures are equal in both cases.

	DRNSE, non-cat. wall			DRNSE, fully-cat. wall			Experiment
#	q [MW/m^2]	St	H_w [MW/kg]	q [MW/m^2]	St	H_w [MW/kg]	q [MW/m^2], ()=St
3.1	13.63	0.0126	-28.442	14.40	0.0125	-29.068	14.11
3.2	15.14	0.0158	-28.370	16.12	0.0156	-29.068	15.26
3.3	34.50	0.0220	-27.345	37.00	0.0216	-28.914	34.51
3.4	32.99	0.0192	-27.381	35.20	0.0189	-29.066	30.26
3.5	27.27	0.0202	-32.243	28.68	0.0197	-33.332	25.00
3.6	26.14	0.0165	-31.967	28.10	0.0163	-33.332	26.31
3.7	4.70	0.0176	-29.065	4.71	0.0176	-29.069	3.70
3.8	14.43	0.0182	-28.539	15.54	0.0180	-29.069	14.00
3.9	1.36	0.0441	-28.210	1.59	0.0445	-29.069	(0.045)
3.10	16.31	0.1137	-22.998	23.64	0.1172	-29.054	21.00
3.11	11.21	0.0823	-26.227	14.40	0.0825	-29.054	15.00

Table 5: Test cases 3.1 - 3.11: Results

It is interesting to note that the Stanton number is hardly influenced by the catalycity of the surface. Nevertheless, the knowledge of the Stanton number alone does not render the wall heat-flux, since the stagnation-point gas-composition — and hence the stagnation enthalpy — is not known a-priori in a non-equilibrium flow. The Stanton number has thus limited value in the analysis of non-equilibrium flows. In the cases 3.10 and 3.11 the DRNSE-results indicate a high catalycity of the surfaces used in the experiments.

8 Conclusions

A useful approximation for the stagnation-streamline quantities in hypersonic blunt-body flows can be obtained from the numerical integration of the dimensionally reduced Navier–Stokes equations. The presented numerical method provides an ideal tool for the investigation of non–equilibrium and near local-equilibrium flows, as it allows a fast, high–resolution calculation of the stagnation-streamline quantities.

Up to now, only chemical non-equilibrium has been investigated in depth. But we are hopeful to achieve similar results for thermal non-equilibrium. First calculations have been performed based on an explicit finite-volume scheme for the DRNSE (cf. [32]). For practical applications however, the implicit scheme used in the present work has to be extended to thermal non-equilibrium.

Investigations for plane two-dimensional flows about cylinders have not been carried out yet. In these flows the shock standoff-distance is larger compared to flows about spheres. It might thus be expected that higher errors in the predictions of the shock standoff-distances and slightly less favorable results for the stagnation-point heat-flux will be found.

9 Figures

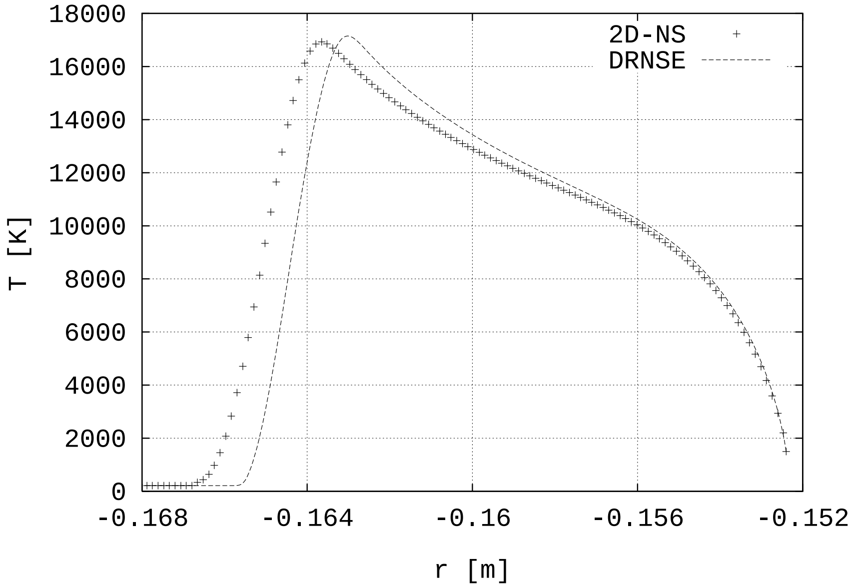

Figure 5: Case 2.1, Temperature

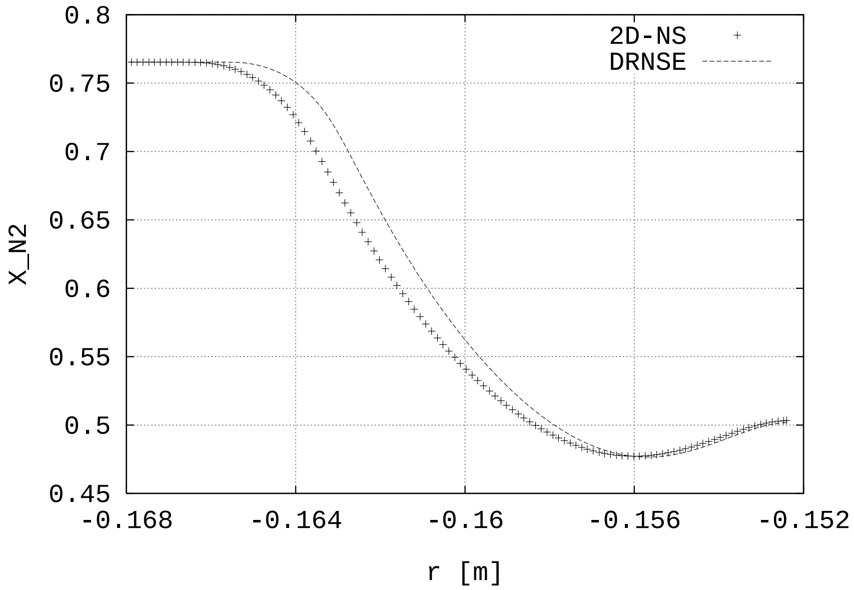

Figure 6: Case 2.1, Mass Fraction of X_{N_2}

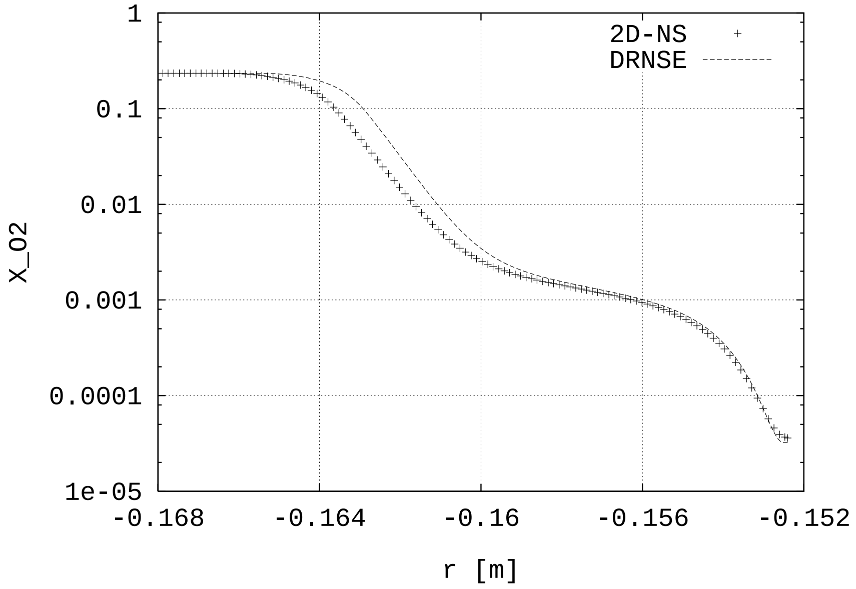

Figure 7: Case 2.1, Mass Fraction of X_{O_2}

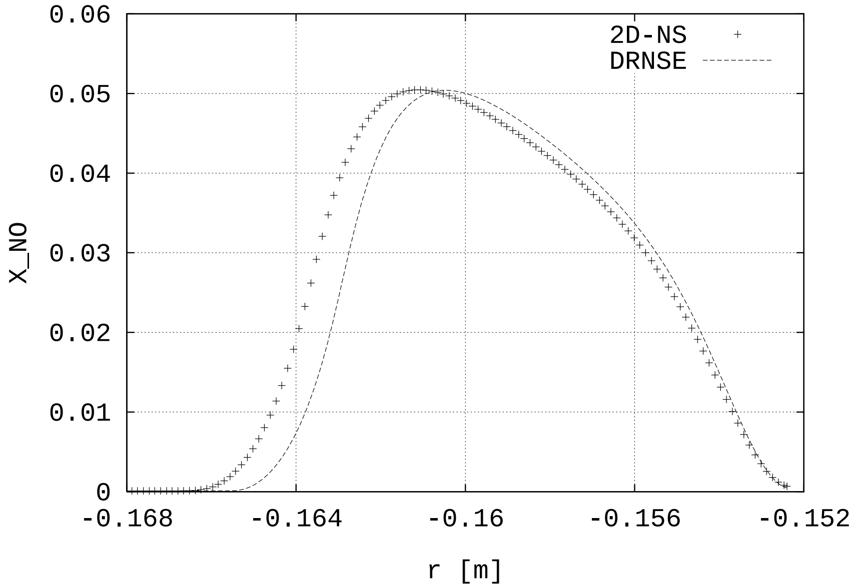

Figure 8: Case 2.1, Mass Fraction of X_{NO}

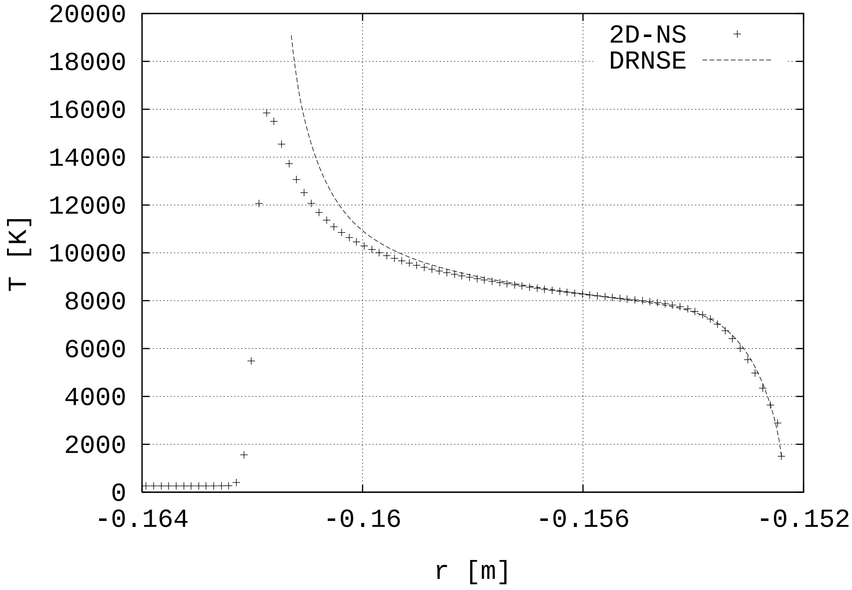

Figure 9: Case 2.2, Temperature

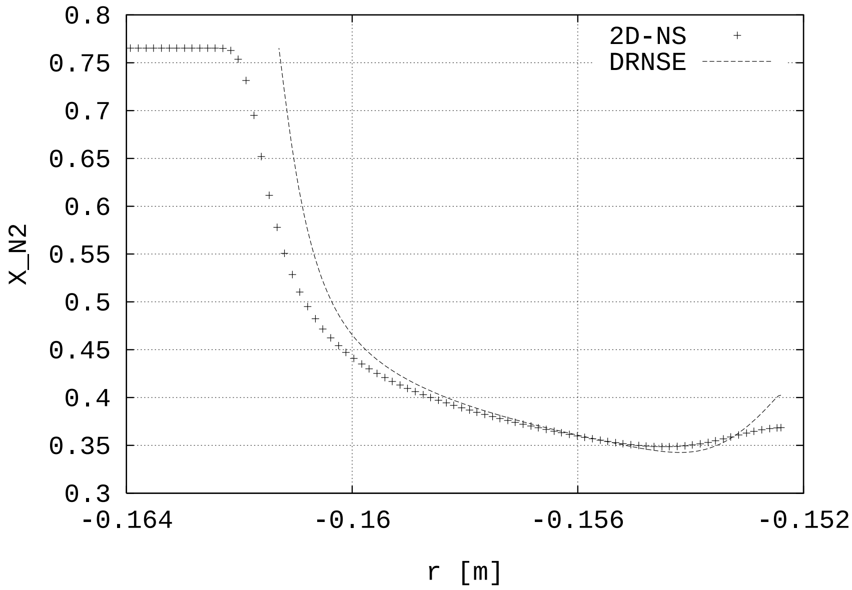

Figure 10: Case 2.2, Mass Fraction of X_{N_2}

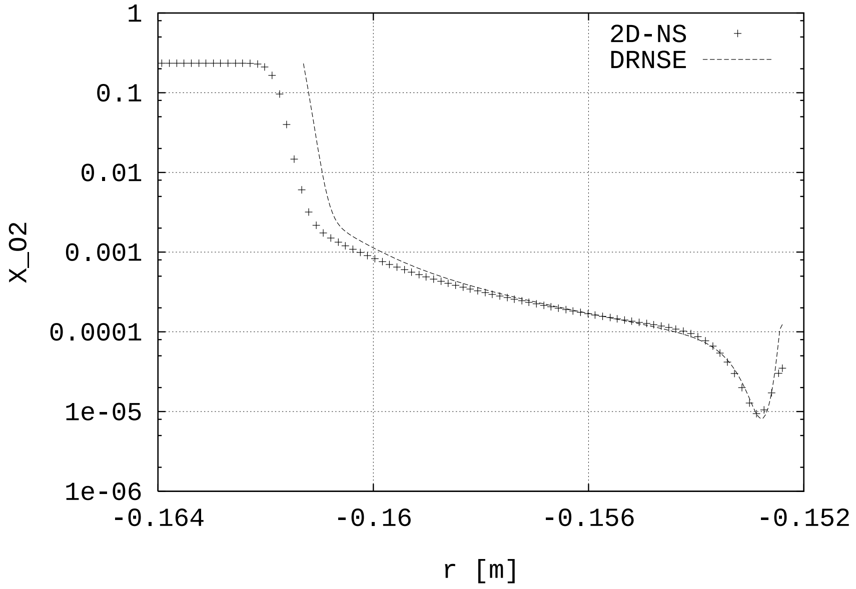

Figure 11: Case 2.2, Mass Fraction of X_{O_2}

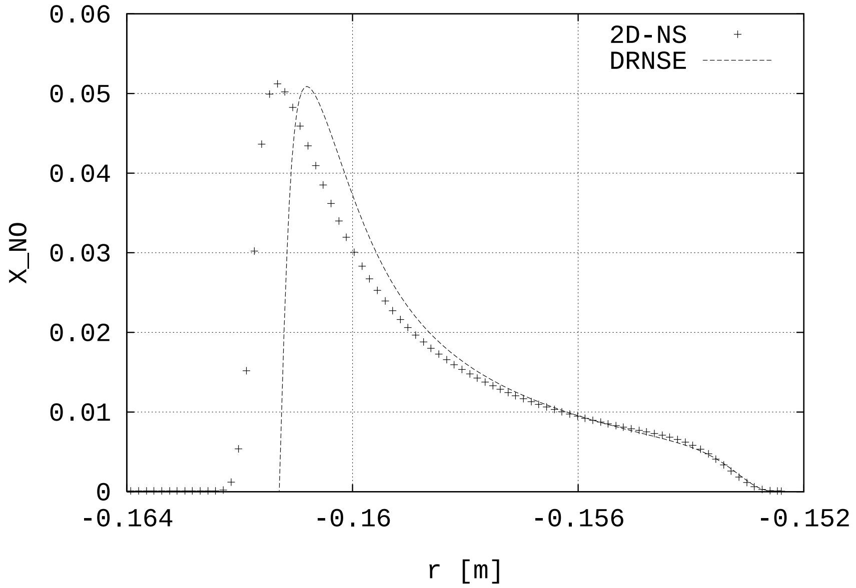

Figure 12: Case 2.2, Mass Fraction of X_{NO}

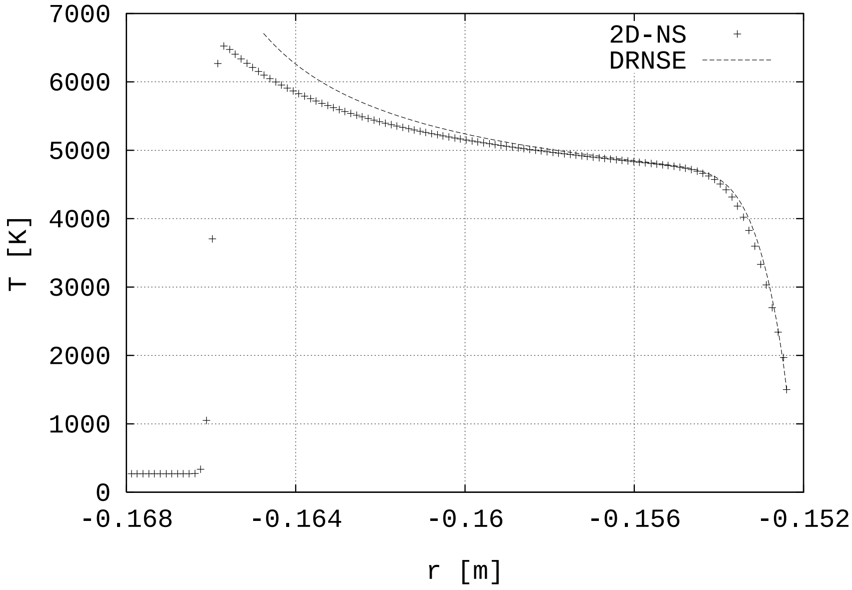

Figure 13: Case 2.3, Temperature

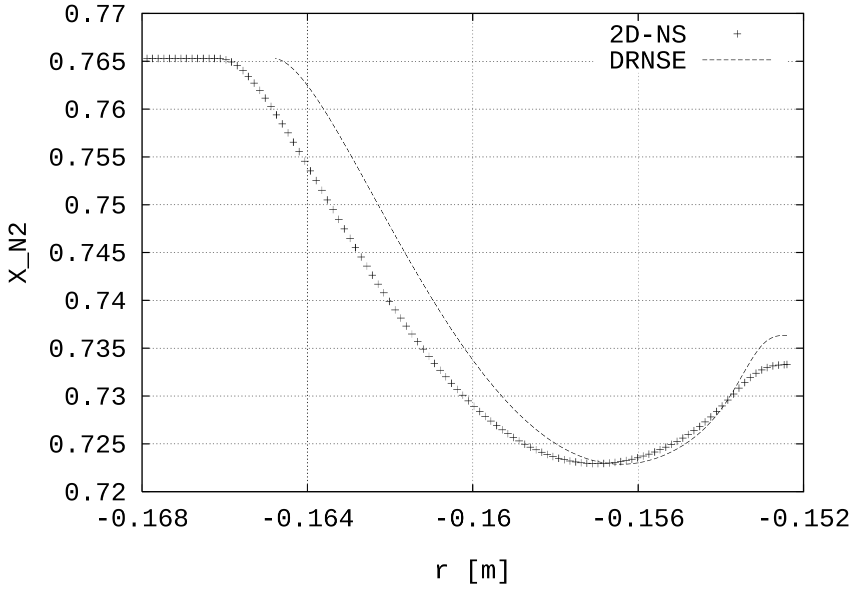

Figure 14: Case 2.3, Mass Fraction of X_{N_2}

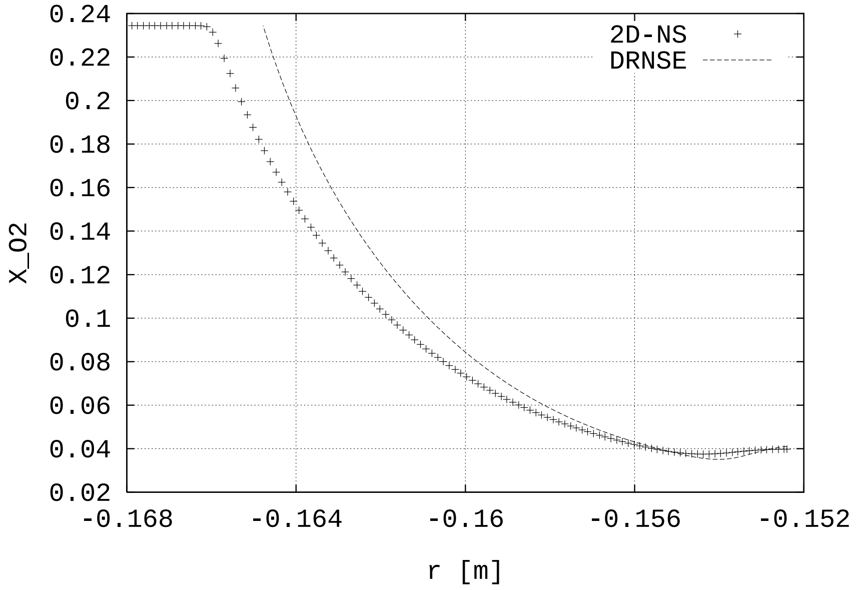

Figure 15: Case 2.3, Mass Fraction of X_{O_2}

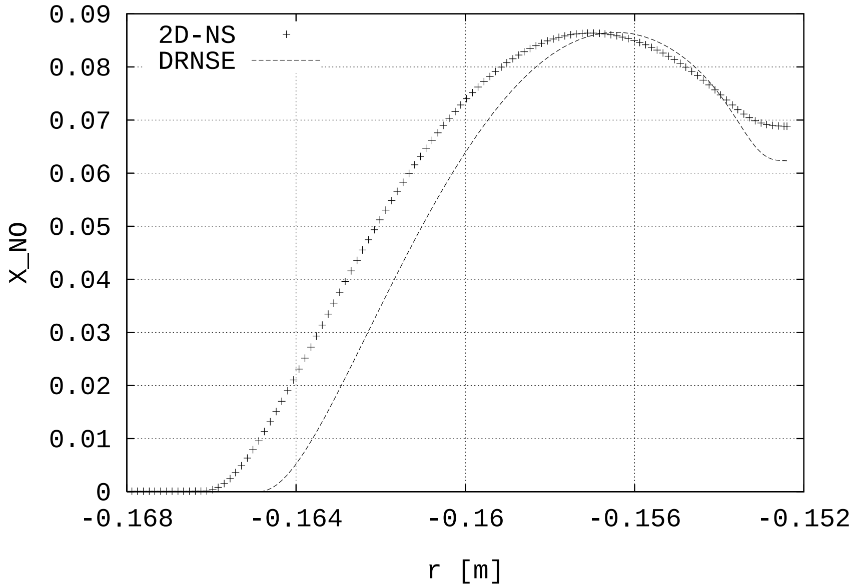

Figure 16: Case 2.3, Mass Fraction of X_{NO}

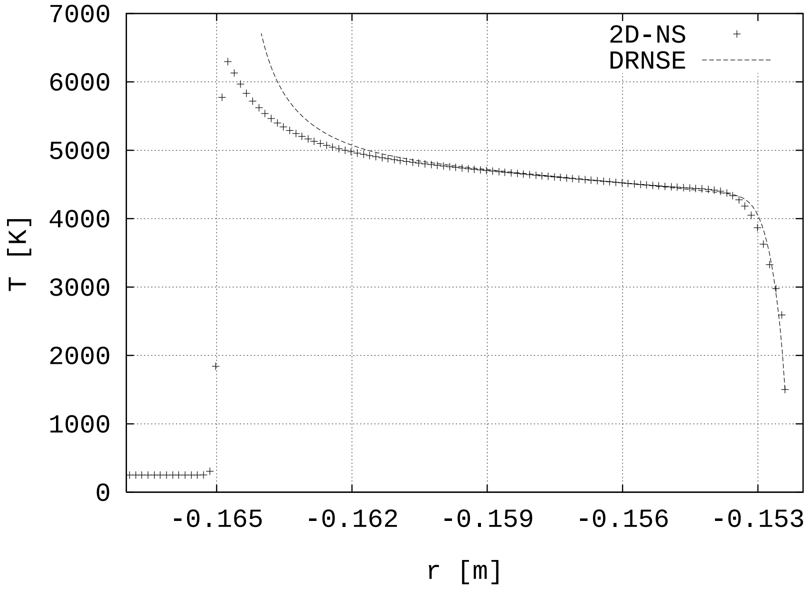

Figure 17: Case 2.4, Temperature

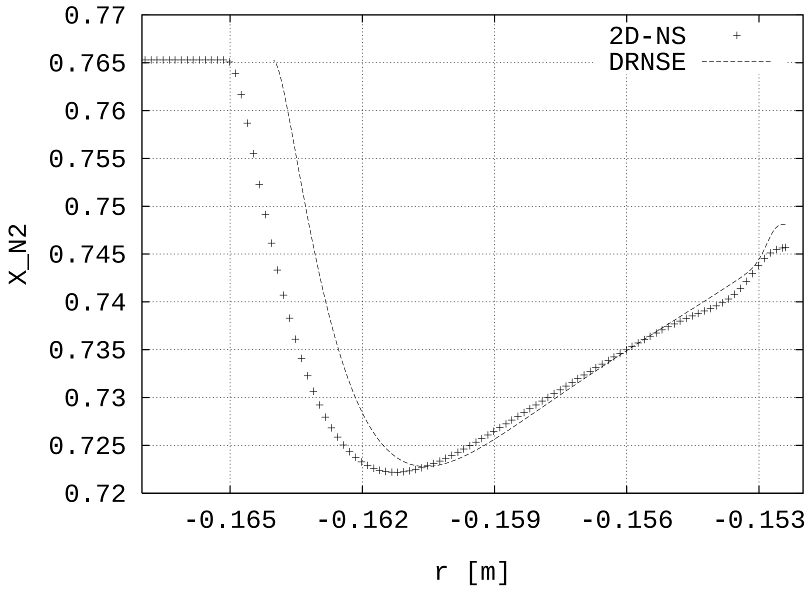

Figure 18: Case 2.4, Mass Fraction of X_{N_2}

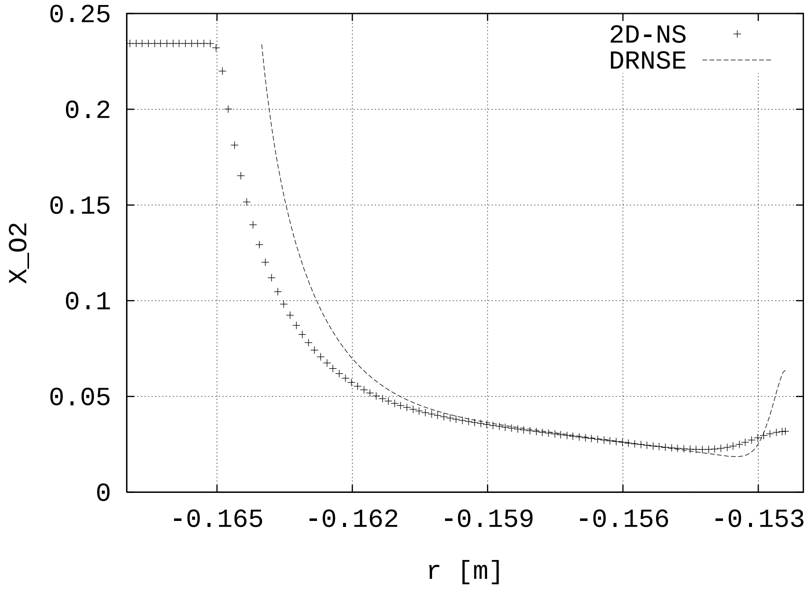

Figure 19: Case 2.4, Mass Fraction of X_{O_2}

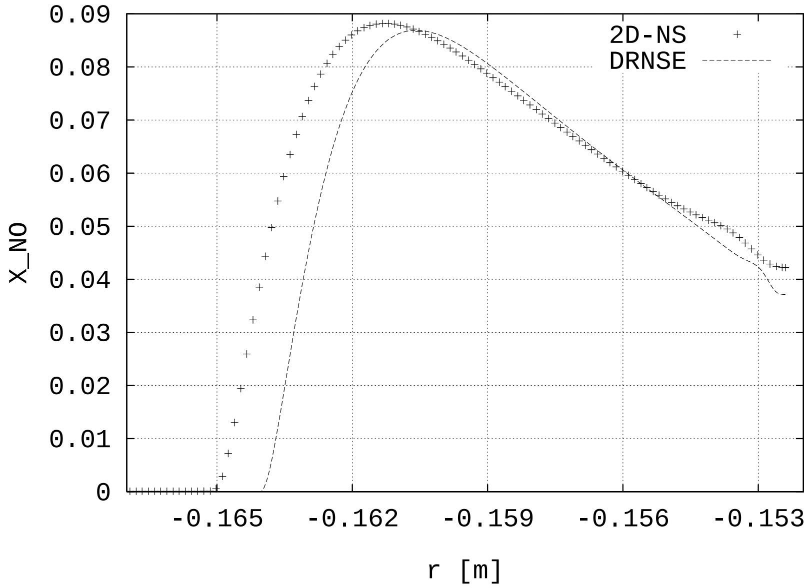

Figure 20: Case 2.4, Mass Fraction of X_{NO}

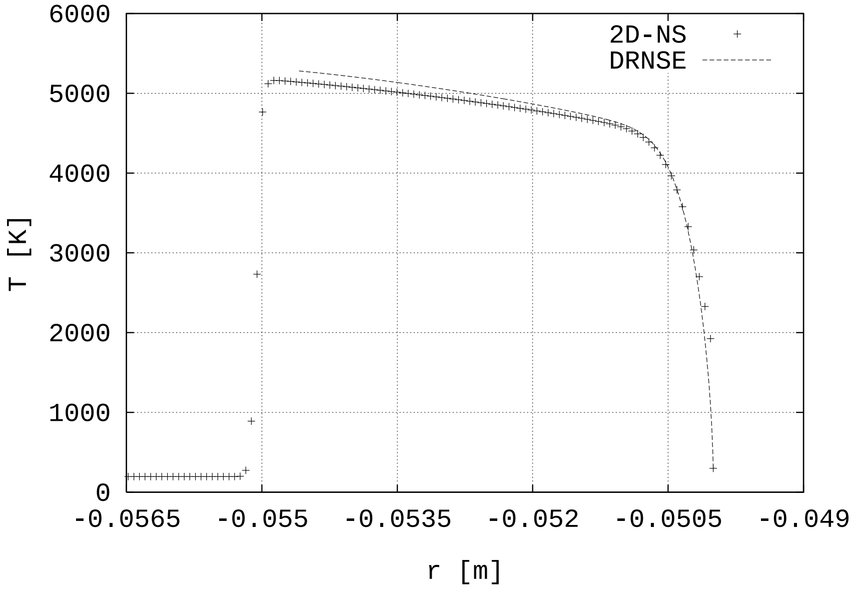

Figure 21: Case 2.5, Temperature

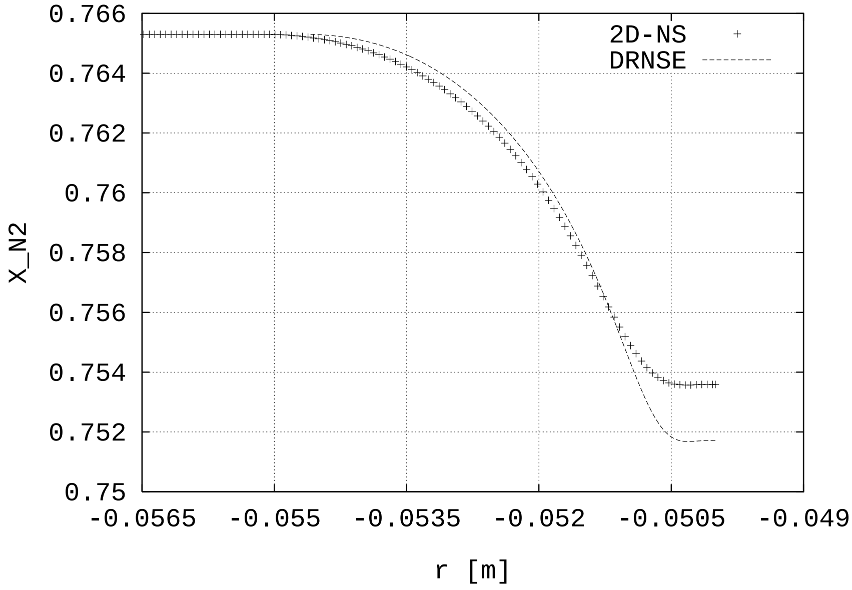

Figure 22: Case 2.5, Mass Fraction of X_{N_2}

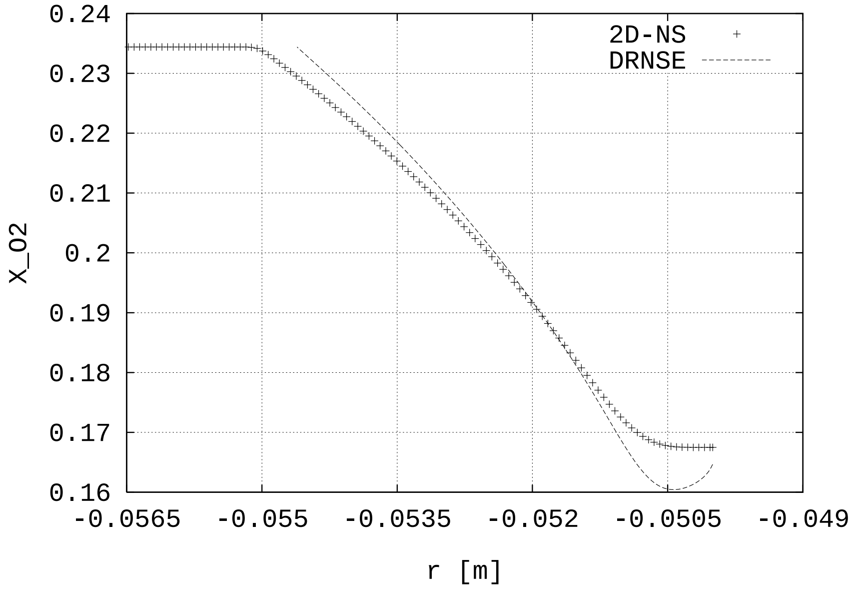

Figure 23: Case 2.5, Mass Fraction of X_{O_2}

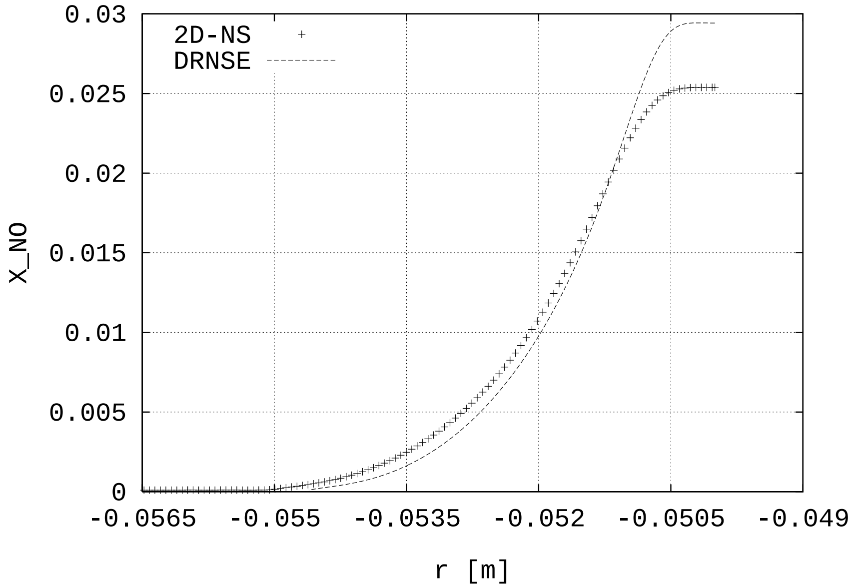

Figure 24: Case 2.5, Mass Fraction of X_{NO}

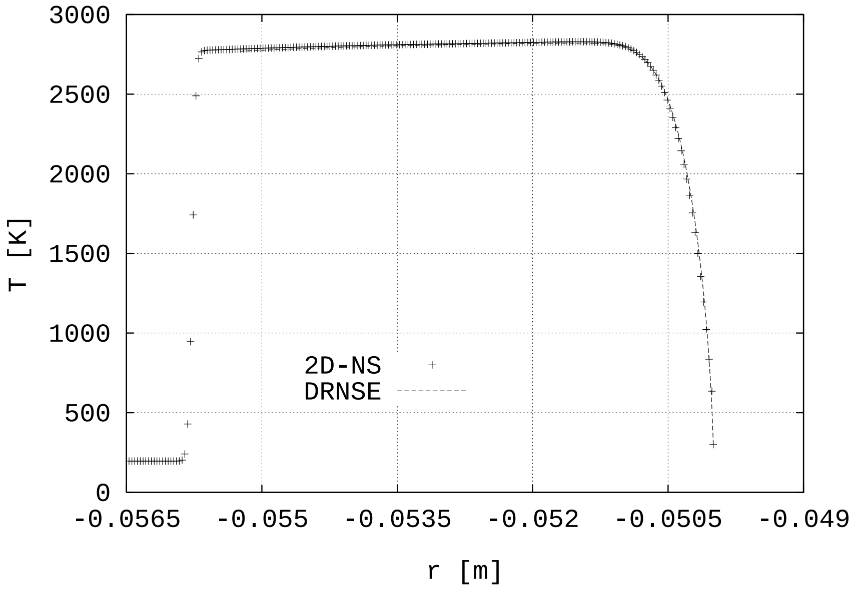

Figure 25: Case 2.6, Temperature

References

[1] Hirschfelder JO, Curtiss CF, Bird RB (1965) Molecular Theory of Gases and Liquids. Wiley

[2] Kao HC (1964) Hypersonic Viscous Flow Near the Stagnation Streamline of a Blunt Body. AIAA J 2: 1892-1897

[3] Metz S (1995) Numerische Verfahren zur Berechnung des Stoff- und Impulstransports in Wasserstoff–Luft und Methan–Luft Gemischen. Dissertation RWTH Aachen, Verlag Shaker Aachen

[4] Wen C, Hornung H (1995) Experiments on Hypervelocity Dissociating Flow over Spheres. In: Proc Internat Symposium on Shock Waves, Marseille, France

[5] Bird RB, Stewart WE, Lightfoot EN (1960) Transport Phenomena. Wiley

[6] Freeman NC (1958) Non-equilibrium flow of an ideal dissociating gas. J. Fluid Mech. 4: 407

[7] Probstein RF, Hayes WD (1966) Hypersonic Flow Theory. Academic Press, 2nd edition

[8] Swigart RJ (1962) A theory of asymmetric hyperbolic blunt body flow. AIAA Journal 1: 1034

[9] Conti RJ (1966) A theoretical study of non-equilibrium blunt body flow. J. Fluid Mech. 24(1): 65–88

[10] Vinokur M (1970) On stagnation-point conditions in non-equilibrium inviscid blunt body flows. J. Fluid Mech. 43: 49–75

[11] Anderson JD (1989) Hypersonic and High Temperature Gas Dynamics. MacGraw-Hill Book Company

[12] Fay JA, Riddell FR (1958) Theory of Stagnation Point Heat Transfer in Dissociated Air. J. Aero. Sci. 25(2): 73–85

[13] Clarke JF, McChesney M (1976) Dynamics of Relaxing Gases. Butterworths

[14] Clarke JF, McChesney M (1964) The Dynamics of Real Gases. Butterworths

[15] Vincenti WG, Kruger ChH (1965) Introduction to Physical Gas Dynamics. John Wiley & Sons Inc.

[16] Marrone PV, Treanor CE (1963) Chemical Relaxation with Preferential Dissociation from Excited Vibrational Levels. Physics of Fluids 6(9): 1215–1221

[17] Park C (1990) Nonequilibrium Hypersonic Aerothermodynamics. Wiley

[18] Park C (1985) On the Convergence of Computation of Chemically Reacting Flows. AIAA 085-0247

[19] Wray KL (1962) Chemical Kinetics of High Temperature Air. Hypersonic Flow Research 7, Riddell FR (Ed.), Academic Press

[20] Zipperer L, Herning F (1936) Beitrag zur Berechnung der Zähigkeit technischer Gasgemische aus den Zähigkeitswerten der Einzelbestandteile. Das Gas- und Wasserfach 4: 49

[21] Stupochenko YV, Losev SA, Osipov AI (1967) Relaxation in Shock Waves, Springer Verlag

[22] Johnston KD, Hendricks WL (1978) A Numerical Solution of the Navier-Stokes Equations for Chemically Nonequilibrium, Merged Stagnation Shock Layers on Spheres abnd Two-Dimensional Cylinders in Air, NASA Technical Paper 1227

[23] Hirschfelder JO (1957) Generalization of the Eucken Correction for Mixtures of Polyatomic Gase. Conference on Thermodynamics and Transport Properties of Fluids July 1957

[24] Klomfass A (1995) Hyperschallströmungen im thermodynamischen Nichtgleichgewicht. Dissertation RWTH Aachen, Verlag Shaker, Aachen

[25] Klomfass A, Müller S, Ballmann J (1993) Modelling of Transport Phenomena for the Hypersonic Stagnation Point Heat Transfer Problem. AIAA-Paper 93-5047

[26] Müller S (1993) NSCNG2 – Ein Programm zur räumlich zweidimensionalen, instationären Strömungssimulation thermisch perfekter aber kalorisch nicht perfekter Gasgemische im chemischen Nichtgleichgewicht. Institut für Geometrie und Praktische Mathematik, RWTH Aachen, Institutsbericht Nr. 89

[27] Müller S, Dickopp Ch, Ballmann J, Jeltsch R (1993) Computation of Viscous Hypersonic Nonequilibrium Blunt Body Flow. ZFW 17: 125–130

[28] Müller S (1993) Erweiterung von ENO–Verfahren auf zwei Raumdimensionen und Anwendung auf hypersonische Staupunktprobleme. Dissertation, RWTH Aachen, Verlag Shaker, Aachen

[29] Vetter M (1993) Hyperschallströmungen von Modellen im Stoßwellenkanal. Dissertation, RWTH Aachen, Verlag Mainz, Wissenschaftsverlag

[30] Olivier H (1995) privat communication, Stoßwellenlabor RWTH Aachen

[31] Eitelberg G, Krek RM (1995) privat communication, DLR Göttingen

[32] Klomfass A, Müller S, Ballmann J (1995) Analysis of Non-Equilibrium Hypersonic Blunt Body Flow with the Local Similarity Method. in: Proc. Int. Symposium on Shock Waves, Pasadena, USA

10 Appendix

10.1 Alternative derivation of the transformation

For those who are not familiar with tensor calculus we will derive the balance equations for rotational symmetric flow from those in cartesian coordinates. The two methods coincide if the coordinate transformation is interpreted as a change of bases.

10.1.1 Transformation to spherical coordinates

We consider the transformation of equation (12) from cartesian into spherical coordinates $\tilde{\mathbf{x}} = (\tilde{x}^1, \tilde{x}^2, \tilde{x}^3)^T = (r, \theta, \phi)^T$ with

$$\begin{aligned} x^1 &= r\cos\phi\sin\theta\,, \\ x^2 &= r\sin\phi\sin\theta\,, \\ x^3 &= r\cos\theta. \end{aligned}$$

The Jacobian of the transformation is

$$\mathbf{G} = \left(\frac{\partial\,\tilde{x}^i}{\partial\,x^k}\right)_{i,k=1,2,3} = \begin{pmatrix} \cos\phi\sin\theta & \sin\phi\sin\theta & \cos\theta \\ \cos\phi\cos\theta/r & \sin\phi\cos\theta/r & -\sin\theta/r \\ -\sin\phi/r\sin\theta & \cos\phi/r\sin\theta & 0 \end{pmatrix},$$

and its inverse

$$\mathbf{G}^{-1} = \left(\frac{\partial\,x^i}{\partial\,\tilde{x}^k}\right)_{i,k=1,2,3} = \begin{pmatrix} \cos\phi\sin\theta & r\cos\phi\cos\theta & -r\sin\phi\sin\theta \\ \sin\phi\sin\theta & r\sin\phi\cos\theta & r\cos\phi\sin\theta \\ \cos\theta & -r\sin\theta & 0 \end{pmatrix}.$$

These matrices are related to the components of the contravariant and the covariant basis vectors as follows

$$\mathbf{G} = \left(\tilde{\mathbf{g}}^1, \tilde{\mathbf{g}}^2, \tilde{\mathbf{g}}^3\right)^T, \quad \mathbf{G}^{-1} = (\tilde{\mathbf{g}}_1, \tilde{\mathbf{g}}_2, \tilde{\mathbf{g}}_3)\,.$$

From these the matrix $\mathbf{M}$ of metrices is calculated as

$$\mathbf{M} = \left(\tilde{\mathbf{g}}^i\tilde{\mathbf{g}}^k\right)_{i,k=1,2,3} = \begin{pmatrix} 1 & 0 & 0 \\ 0 & r^{-2} & 0 \\ 0 & 0 & (r\sin\theta)^{-2} \end{pmatrix}.$$

The vector $\tilde{\mathbf{v}} = (\tilde{v}^1, \tilde{v}^2, \tilde{v}^3)^T$ of the velocity components in spherical coordinates is related to the vector $\mathbf{v} = (v^1, v^2, v^3)^T$ of the velocity components in cartesian coordinates by

$$\mathbf{v} = \mathbf{G}^{-1}\tilde{\mathbf{v}} \quad \text{respectively} \quad \tilde{\mathbf{v}} = \mathbf{G}\mathbf{v}\,.$$

For arbitrary scalar functions $\Psi = \Psi(t, \underset{\sim}{x})$, vector–valued functions $\mathbf{f} = \mathbf{f}(t, \underset{\sim}{x}) = (f_1, f_2, f_3)^T$ and matrix–valued functions $\mathbf{A} = \mathbf{A}(t, \underset{\sim}{x}) = (a_{ij})_{i,j=1,2,3}$ we define the divergence and the gradient with respect to the components of an arbitrary coordinate vector $\mathbf{x}$ as

$$\text{grad}_{\mathbf{x}}\, \Psi = \left(\frac{\partial\, f}{\partial\, x_1}, \frac{\partial\, f}{\partial\, x_2}, \frac{\partial\, f}{\partial\, x_3} \right)^T, \quad \text{div}_{\mathbf{x}}\, \mathbf{f} = \sum_{i=1}^{3} \frac{\partial\, f_i}{\partial\, x_i}, \tag{93}$$

$$\text{div}_{\mathbf{x}}\, \mathbf{A} = \begin{pmatrix} \sum_{i=1}^{3} \frac{\partial\, a_{1i}}{\partial\, x_i} \\ \sum_{i=1}^{3} \frac{\partial\, a_{2i}}{\partial\, x_i} \\ \sum_{i=1}^{3} \frac{\partial\, a_{3i}}{\partial\, x_i} \end{pmatrix} = \begin{pmatrix} \text{div}_{\mathbf{x}}\, (a_{11}, a_{12}, a_{13})^T \\ \text{div}_{\mathbf{x}}\, (a_{21}, a_{22}, a_{23})^T \\ \text{div}_{\mathbf{x}}\, (a_{31}, a_{32}, a_{33})^T \end{pmatrix}. \tag{94}$$

Then the divergence and gradient terms in (1) to (10) can be transformed as follows:

The divergence of the advection of any scalar quantity Ψ in spherical coordinates is given by

$$\text{div}\, (\Psi \underset{\sim}{v}) = \text{div}_{\tilde{\mathbf{x}}}\, (\Psi \tilde{\mathbf{v}}) + 2\Psi \tilde{v}^1/r + \Psi \tilde{v}^2 \cot\theta \tag{95}$$

where Ψ is any of the quantities $\rho_i,\ \rho,\ \rho H,\ \epsilon^\alpha$ and unity. The divergence of the hydrostatic pressure takes the form

$$\text{div}\, (p \underset{\approx}{E}) = \mathbf{G}^{-1}\mathbf{M}\ \text{grad}_{\tilde{\mathbf{x}}}\, (p) = \mathbf{G}^{-1}\text{div}_{\tilde{\mathbf{x}}}\, (p\ \mathbf{M}). \tag{96}$$

The divergence of the advection of the momentum is given by

$$\text{div}\, (\rho \underset{\sim}{\tilde{v}} \circ \underset{\sim}{\tilde{v}}) = \mathbf{G}^{-1} \left(\text{div}_{\tilde{\mathbf{x}}}\, (\rho \tilde{\mathbf{v}} \tilde{\mathbf{v}}^T) + \rho \mathbf{A} \tilde{\mathbf{v}} \right) \tag{97}$$

with

$$\mathbf{A} = \begin{pmatrix} 2\tilde{v}^1/r & \tilde{v}^1 \cot\theta - r\tilde{v}^2 & -r\tilde{v}^3 \sin^2\theta \\ 4\tilde{v}^2/r & \tilde{v}^2 \cot\theta & -\tilde{v}^3 \cos\theta \sin\theta \\ 4\tilde{v}^3/r & 3\tilde{v}^3 \cot\theta & 0 \end{pmatrix}.$$

The divergence of the shear stress tensor now reads

$$\text{div}\, (\underset{\approx}{\tau}) = \mathbf{G}^{-1} \left(\text{div}_{\tilde{\mathbf{x}}}\, (\tilde{\boldsymbol{\tau}}) + \mathbf{M}^{1/2} \boldsymbol{\alpha}\, r^{-1} \right) \tag{98}$$

with

$$\boldsymbol{\alpha} = \begin{pmatrix} 2\tilde{\tau}^{11} + \tilde{\tau}^{12} r \cot\theta - \tilde{\tau}^{22} r^2 - \tilde{\tau}^{33} r^2 \sin^2\theta \\ 4\tilde{\tau}^{12} r + \tilde{\tau}^{22} r^2 \cot\theta - \tilde{\tau}^{33} r^2 \cos\theta \sin\theta \\ 4\tilde{\tau}^{13} r \sin\theta + 3\tilde{\tau}^{23} r^2 \cos\theta \end{pmatrix}.$$

Herein, the contravariant components of the transformed stress tensor are

$$
\begin{aligned}
\tilde{\tau}^{11} &= -2\mu\left(\tilde{v}^1_{,r} - \frac{1}{3}\mathrm{div}\,\underset{\sim}{\tilde{v}}\right)\,,\\
\tilde{\tau}^{12} &= -\mu\left(\tilde{v}^2_{,r} + \tilde{v}^1_{,\theta}\frac{1}{r^2}\right)\,,\\
\tilde{\tau}^{13} &= -\mu\left(\tilde{v}^3_{,r} + \tilde{v}^1_{,\phi}\frac{1}{(r\sin\theta)^2}\right)\,,\\
\tilde{\tau}^{22} &= -2\mu\left(\tilde{v}^2_{,\theta} + \frac{\tilde{v}^1}{r} - \frac{1}{3}\mathrm{div}\,\underset{\sim}{\tilde{v}}\right)\frac{1}{r^2}\,,\\
\tilde{\tau}^{23} &= -\mu\left(\tilde{v}^3_{,\theta} + \tilde{v}^2_{,\phi}\frac{1}{\sin^2\theta}\right)\frac{1}{r^2}\,,\\
\tilde{\tau}^{33} &= -2\mu\left(\frac{\tilde{v}^1}{r} + \tilde{v}^2\cot\theta + \tilde{v}^3_{,\phi} - \frac{1}{3}\mathrm{div}\,\underset{\sim}{\tilde{v}}\right)\frac{1}{(r\sin\theta)^2}.
\end{aligned}
$$

The viscous dissipation term now reads

$$
\mathrm{div}\,(\underset{\approx}{\tau}\underset{\sim}{v}) = \mathrm{div}_{\tilde{\mathbf{x}}}\,(\tilde{\boldsymbol{\tau}}\,\mathbf{M}^{-1}\tilde{\mathbf{v}}) + a\,r^{-1} - b\,r \tag{99}
$$

with

$$
\begin{aligned}
a &= 2\tilde{v}^1\tilde{\tau}^{11} + \tilde{v}^1\tilde{\tau}^{12}r\cot\theta + 4\tilde{v}^2\tilde{\tau}^{12}r^2 + \tilde{v}^2\tilde{\tau}^{22}r^3\cot\theta + \\
&\quad 4\tilde{v}^3\tilde{\tau}^{13}r^2\sin^2\theta + 3\tilde{v}^3\tilde{\tau}^{23}r^3\sin\theta\cos\theta\,,\\
b &= 2\tilde{v}^2\tilde{\tau}^{21} + 2\tilde{v}^3\tilde{\tau}^{31}\sin^2\theta + 2\tilde{v}^3\tilde{\tau}^{32}r\sin\theta\cos\theta.
\end{aligned}
$$

In the evaluation of the heat and diffusion fluxes (7), (10) and (9) the divergence of certain gradients has to be calculated. Any gradient of a scalar quantity ω transforms as follows

$$
\mathrm{grad}\,\omega = \mathbf{M}\;\mathrm{grad}_{\tilde{\mathbf{x}}}\,\omega. \tag{100}
$$

Define $\underset{\sim}{q} = \Psi\mathrm{grad}\,\omega$ where Ψ is another scalar quantity. The divergence of this vector is given by

$$
\mathrm{div}\,\underset{\sim}{q} = \mathrm{div}_{\tilde{\mathbf{x}}}\,\tilde{\mathbf{q}} + 2q^1/r + q^2\cot\theta \tag{101}
$$

where $\tilde{\mathbf{q}}$ is given by

$$
\tilde{\mathbf{q}} = \Psi\mathbf{M}\;\mathrm{grad}_{\tilde{\mathbf{x}}}\,\omega. \tag{102}
$$

Substituting the above transformations in the equations of balance we get the representation in spherical coordinates. There, the equations of momentum are multiplied by $\mathbf{G}$ from the left. This renders the equations for the components of the momentum $\rho\tilde{v}^1, \rho\tilde{v}^2, \rho\tilde{v}^3$ in spherical coordinates.

10.1.2 Variable transformation

To get a more compact representation of the balance equations some further transformations are introduced by engineers, see e.g. Bird, Stewart and Lightfood [5]. There, all the transformations are written in terms of tensor calculus. These coincide with the formulas we derived in the previous section, if we define the following quantities:

$$v_r = v^1,\; v_\theta = v^2 r,\; v_\phi = v^3 r\sin\theta\,,$$

$$\begin{array}{lll} \tau_{rr} = \tilde\tau^{11}\,, & \tau_{\theta\theta} = \tilde\tau^{22}r^2\,, & \tau_{\theta\phi} = \tilde\tau^{23}r^2\sin\theta\,, \\ \tau_{r\theta} = \tilde\tau^{12}r\,, & \tau_{r\phi} = \tilde\tau^{13}r\sin\theta\,, & \tau_{\phi\phi} = \tilde\tau^{33}r^2\sin^2\theta\,, \end{array}$$

$$q_r = q^1,\; q_\theta = q^2 r,\; q_\phi = q^3 r\sin\theta\,.$$

In matrix–vector–representation these transformations can be written as

$$\mathbf{v} = \mathbf{M}^{-1/2}\tilde{\mathbf{v}},\; \boldsymbol{\tau}\; = \mathbf{M}^{-1/2}\tilde{\boldsymbol{\tau}}\mathbf{M}^{-1/2},\; \mathbf{q} = \mathbf{M}^{-1/2}\tilde{\mathbf{q}}$$

with

$$\mathbf{v} = (v_r, v_\theta, v_\phi)^T,\; \mathbf{q} = (q_r, q_\theta, q_\phi)^T.$$

Then the transformation of the divergences and gradients (95) to (102) results in:

$$\begin{aligned} \operatorname{div}(\Psi\underset{\sim}{v}) &= \operatorname{div}_{\tilde{\mathbf{x}}}(\Psi\mathbf{M}^{1/2}\mathbf{v}) + \Psi(2v_r + v_\theta\cot\theta)r^{-1}\,, \\ \operatorname{div}(p\underset{\approx}{E}) &= \mathbf{G}^{-1}\mathbf{M}^{1/2}\operatorname{div}_{\tilde{\mathbf{x}}}(\mathbf{M}^{1/2}p)\,, \\ \operatorname{div}(\rho\underset{\sim}{\tilde v}\circ\underset{\sim}{\tilde v}) &= \mathbf{G}^{-1}\mathbf{M}^{1/2}\left(\operatorname{div}_{\tilde{\mathbf{x}}}(\rho\mathbf{M}^{1/2}\mathbf{v}\mathbf{v}^T) + \rho\,\boldsymbol{\beta}\,r^{-1}\right)\,, \\ \operatorname{div}(\underset{\approx}{\tau}) &= \mathbf{G}^{-1}\mathbf{M}^{1/2}\left(\operatorname{div}_{\tilde{\mathbf{x}}}(\boldsymbol{\tau}\mathbf{M}^{1/2}) + \boldsymbol{\alpha}\,r^{-1}\right)\,, \\ \operatorname{div}(\underset{\approx}{\tau}\underset{\sim}{v}) &= \operatorname{div}_{\tilde{\mathbf{x}}}(\mathbf{M}^{1/2}\boldsymbol{\tau}\mathbf{v}) + \gamma\,r^{-1}\,, \\ \operatorname{grad}\omega &= \mathbf{M}^{1/2}\operatorname{grad}_{\tilde{\mathbf{x}}}\omega\,, \\ \operatorname{div}\underset{\sim}{q} &= \operatorname{div}_{\tilde{\mathbf{x}}}\mathbf{q} + (2q_r + q_\theta\cot\theta)r^{-1},\; \mathbf{q} = \Psi\mathbf{M}^{1/2}\operatorname{grad}_{\tilde{\mathbf{x}}}\omega \end{aligned}$$

with

$$\boldsymbol{\alpha} = \begin{pmatrix} 2\tau_{rr} - \tau_{\theta\theta} - \tau_{\phi\phi} + \tau_{r\theta}\cot\theta \\ 3\tau_{r\theta} + (\tau_{\theta\theta} - \tau_{\phi\phi})\cot\theta \\ 3\tau_{r\phi} + 2\tau_{\theta\phi}\cot\theta \end{pmatrix},\; \boldsymbol{\beta} = \begin{pmatrix} 2v_r^2 + v_r v_\theta\cot\theta - v_\theta^2 - v_\phi^2 \\ 3v_r v_\theta + v_\theta^2\cot\theta - v_\phi^2\cot\theta \\ 3v_r v_\phi + 2v_\theta v_\phi\cot\theta \end{pmatrix},$$

$$\gamma = 2(v_r\tau_{rr} + v_\theta\tau_{r\theta} + v_\phi\tau_{r\phi}) + (v_r\tau_{r\theta} + v_\theta\tau_{\theta\theta} + v_\phi\tau_{\theta\phi})\cot\theta.$$

The contravariant components of the shear stress tensor read

$$
\begin{aligned}
\tau_{rr} &= -\mu\left\{\frac{4}{3}v_{r,r}-\frac{2}{3}\frac{v_{\theta,\theta}}{r}-\frac{2}{3}\frac{v_{\phi,\phi}}{r\sin\theta}-\frac{4}{3}\frac{v_r}{r}-\frac{2}{3}\frac{v_\theta\cot\theta}{r}\right\}, \\
\tau_{r\theta} &= -\mu\left\{v_{\theta,r}+\frac{v_{r,\theta}}{r}-\frac{v_\theta}{r}\right\}, \\
\tau_{r\phi} &= -\mu\left\{v_{\phi,r}-\frac{v_\phi}{r}+\frac{v_{r,\phi}}{r\sin\theta}\right\}, \\
\tau_{\theta\theta} &= -\mu\left\{\frac{4}{3}\frac{v_{\theta,\theta}}{r}-\frac{2}{3}v_{r,r}-\frac{2}{3}\frac{v_r}{r}-\frac{2}{3}\frac{v_\theta\cot\theta}{r}\right\}, \\
\tau_{\theta\phi} &= -\mu\left\{\frac{v_{\phi,\theta}}{r}+\frac{v_{\theta,\phi}}{r\sin\theta}-\frac{v_\phi\cot\theta}{r}\right\}, \\
\tau_{\phi\phi} &= -\mu\left\{\frac{4}{3}\frac{v_{\phi,\phi}}{r\sin\theta}-\frac{2}{3}\frac{v_{\theta,\theta}}{r}-\frac{2}{3}v_{r,r}+\frac{2}{3}\frac{v_r}{r}+\frac{4}{3}\frac{v_\theta\cot\theta}{r}\right\}.
\end{aligned}
$$

10.1.3 Rotational symmetry

In the case of a rotational geometry the flow field is inherently rotational, i.e.

$$v_\phi \equiv 0 \text{ and } \frac{\partial}{\partial\,\phi} \equiv 0\,.$$

Thus, the derivatives with respect to θ can be neglected in the definition of the divergence and gradient (93, 94) as well as the equation for the angular momentum. The quantities $\boldsymbol{\alpha}$, $\boldsymbol{\beta}$ and γ simplify to

$$
\boldsymbol{\alpha} = \begin{pmatrix} 2\tau_{rr}-\tau_{\theta\theta}-\tau_{\phi\phi}+\tau_{r\theta}\cot\theta \\ 3\tau_{r\theta}+(\tau_{\theta\theta}-\tau_{\phi\phi})\cot\theta \\ 0 \end{pmatrix},\quad
\boldsymbol{\beta} = \begin{pmatrix} 2v_r^2+v_r v_\theta\cot\theta-v_\theta^2 \\ 3v_r v_\theta+v_\theta^2\cot\theta \\ 0 \end{pmatrix},
$$

$$\gamma = 2(v_r\tau_{rr}+v_\theta\tau_{r\theta})+(v_r\tau_{r\theta}+v_\theta\tau_{\theta\theta})\cot\theta.$$

The contravariant components of the shear stress tensor now read

$$
\begin{aligned}
\tau_{rr} &= -\mu\left\{\frac{4}{3}v_{r,r}-\frac{2}{3}\frac{v_{\theta,\theta}}{r}-\frac{4}{3}\frac{v_r}{r}-\frac{2}{3}\frac{v_\theta\cot\theta}{r}\right\}, \\
\tau_{r\theta} &= -\mu\left\{v_{\theta,r}+\frac{v_{r,\theta}}{r}-\frac{v_\theta}{r}\right\}, \\
\tau_{\theta\theta} &= -\mu\left\{\frac{4}{3}\frac{v_{\theta,\theta}}{r}-\frac{2}{3}v_{r,r}-\frac{2}{3}\frac{v_r}{r}-\frac{2}{3}\frac{v_\theta\cot\theta}{r}\right\}, \\
\tau_{\phi\phi} &= -\mu\left\{-\frac{2}{3}\frac{v_{\theta,\theta}}{r}-\frac{2}{3}v_{r,r}+\frac{2}{3}\frac{v_r}{r}+\frac{4}{3}\frac{v_\theta\cot\theta}{r}\right\}, \\
\tau_{r\phi} &= \tau_{\theta\phi} = 0.
\end{aligned}
$$

10.2 Wall heat flux estimation due to Fay & Riddell

According to Fay and Riddell [12] the wall heat flux for a spherical and a cylindrical nose can be approximated by

$$q_w = K\,(\rho_e \mu_e)^{0.4} (\rho_w \mu_w)^{0.1} \sqrt{\left(\frac{\partial v}{\partial y}\right)_s} (H_e - H_w) \left[1 + L\,\frac{H_D}{H_e}\right]$$

with

$$L = \begin{cases} (Le)^{0.52} - 1 & , \text{ equilibrium boundary layer} \\ (Le)^{0.63} - 1 & , \text{ frozen boundary layer with a fully catalytic wall} \\ 0 & , \text{ frozen boundary layer with a non-catalytic wall} \end{cases}$$

$$K = \begin{cases} 0.76\,(Pr)^{-0.6} & , \text{ spherical nose} \\ 0.57\,(Pr)^{-0.6} & , \text{ cylindrical nose} \end{cases}$$

where H_D is the diffusion enthalpy given by

$$H_D = \sum_{\alpha=1}^{K} x_{\alpha_e} e_\alpha^0$$

and the stagnation point velocity gradient $(\partial v/\partial y)_s$ is taken from a two-dimensional inviscid calculation. Subscript e denotes the value of a quantity at the outer edge of the boundary layer. In our calculations we have taken the values from the inviscid calculation in the stagnation point. According to the assumption of a constant Prandtl number the Lewis number is just unity.

The data used in Fay & Riddell's formula for test cases 1.1 - 1.20 and 2.1 - 2.6 are presented in table 6 and 7.

Test cases: perfect gas, Source: Exact res./2d-Euler				
Ma	T_w [K]	T_e/T_∞	p_e/p_∞	$(\partial v/\partial y)_s$ [1/s]
2	300	1.8	5.6	5455
5	300	6.0	32.7	12360
10	300	21	129.2	21007
20	300	81	515.5	42051
50	300	81	3219	107790

Table 6: Data used in Fay & Riddell's formula for test cases 1.1 to 1.20

Test cases: chemical-nonequilibrium flows, Source: DRNSE (Euler b/c)									
#	T_w [K]	T_e[K]	p_e[Pa]	$x_{N,e}$	$x_{N_2,e}$	$x_{O,e}$	$x_{O_2,e}$	$x_{NO,e}$	$(\partial v/\partial y)_s$ [1/s]
2.1	1500	10000	3750	.475	.0	.020	.275	.23	26902
2.2	1500	7552	29345	.350	.0	.005	.412	.23	24606
2.3	1500	4506	15530	.729	.037	.074	.001	.16	14435
2.4	1500	4418	61013	.739	.022	.050	.002	.18	12470
2.5	300	4585	19065	.755	.173	.021	.000	.05	44000
2.6	300	2804	9351	.765	.234	.000	.000	.00	31000

Table 7: Data used in Fay & Riddell's formula for test cases 2.1 to 2.6